Aluminum Nitride SAW Resonators

by

Ali Mojdeh

A thesis
presented to the University of Waterloo
in fulfillment of the
thesis requirement for the degree of
Master of Applied Science
in
Electrical and Computer Engineering

Waterloo, Ontario, Canada, 2017

© Ali Mojdeh 2017

AUTHOR'S DECLARATION

I hereby declare that I am the sole author of this thesis. This is a true copy of the thesis, including any required final revisions, as accepted by my examiners.

I understand that my thesis may be made electronically available to the public.

Abstract

Numerous devices need filters for capturing signals and then conditioning them in communications and wireless systems. For several decades, microwave filters have been the center of attention for this type of signal conditioning. However, acoustic filters have recently been gaining attention, mainly because of their miniature size and high quality factor.

Among the various different types of acoustic filters, SAW filters with only metal layers on top of the piezoelectric substrate are studied in this work. The piezoelectric material used in this thesis is aluminum nitride, which exhibits a higher quality factor in SAW resonators compared to lithium niobate or other piezoelectric materials.

An extensive analysis of SAW structures is carried out here, along with an investigation into the relationship between physical dimensions, piezoelectric properties and filter specifications. The proposed design procedure is followed, after which the design is verified by simulation tools such as COMSOL and Coventorware, several prototype units for resonators and filters are fabricated through MEMSCAP.

The tests were performed at the Center for Integrated RF Engineering (CIRFE) lab at the University of Waterloo, Waterloo, Ontario, Canada. The Q factor of the designed aluminum nitride resonator was proven to be higher than that of lithium niobate resonators. The results obtained demonstrate the feasibility of realizing aluminum nitride-based SAW resonators using a commercially available fabrication process from MEMSCAP.

Acknowledgements

I would like to express my greatest gratitude to my supervisor, Professor Raafat R. Mansour, for his constant assistance and inspiration throughout the course of my Master of Applied Sciences studies. It was an honor for me to have the opportunity to work with him. I learned so much from him during my time in the group.

I also wish to thank Dr. Miraftab for his amazing comments and insights on this thesis. As well, my warm gratitude is extended to Dr. Ramahi for his time and effort spent reviewing my work.

It was an amazing opportunity for me to be a member of the Center for Integrated RF Engineering at the University of Waterloo. I want to especially thank the former CIRFE lab manager, Bill Jolley, for his support and help, Dr. Siamak Fouladi and Dr. Mostafa Azizi for their great insights and valuable points, Mitra Nasresfahani for her collaboration and insights, and Ahmed Abdel Aziz for helping me set up the post-processes in the clean room.

Thanks also go to my friends Farzad Yazdani, Tejinder Singh, Johhny Jia and Arash Fouladi for their support, and I would like to extend my gratitude to all members of the CIRFE lab.

My special thanks go to my friend, colleague and office mate, Frank Jiang, for the wonderful two years we had together in the office, his insights and helpful guidance, and the hours he spent with me in the lab.

I also wish to thank my parents for their endless and unconditional help and support all through my life, both academic and personal.

Last but not least, my most special thanks and gratitude go to my beloved wife, Parisa. In the years we had together, everything became sweeter and brighter and without a single doubt, this MASc would not have been completed without her love, support and encouragement.

Dedication

To my loving wife, Parisa, whose warm presence and love helped me succeed.

تقدیم به پدر و مادر عزیزم برای حمایت ها و دعاهای بی دریغشان در تمام ادوار زندگی ام، حتی با وجود فاصله ی زیاد.

To my parents, for their reassurance, prayers and support that made me feel close to them even though they were so far away.

فضای هر ظرفی در اثر محتوای خود تنگ‌تر می‌شود مگر ظرف دانش که با تحصیل علوم، فضای آن بازتر می‌گردد. علی بن ابی طالب (ع)

Arabic Translation: كُلُّ وِعاءٍ يَضيقُ بِما جُعِلَ فيهِ إلاّ وِعاءُ العِلمِ فَإِنَّهُ يَتَّسِعُ بِهِ؛ علی بن ابی طالب (ع)

Every barrel’s capacity gets reduced when one puts things in it, except the barrel of science, which gets less full by obtaining more knowledge. Ali Ibn Abi Taleb (PBUH).

Table of Contents

AUTHOR'S DECLARATION ii
Abstract iii
Acknowledgements iv
Dedication v
List of Figures viii
List of Tables xi
Chapter 1 Introduction 1
1.1 Motivation 1
1.2 Objectives 1
1.3 Thesis Outline 1
Chapter 2 Literature Review 2
2.1 Introduction 2
2.2 Surface Acoustic Wave Resonators 3
2.3 Aluminum Nitride SAW Resonator 10
2.4 Finite Element Analysis of SAW 12
2.5 Tunable SAW Filter 15
Chapter 3 PiezoMUMPs Process 20
3.1 Introduction 20
3.2 Fabrication Process 21
Chapter 4 Simulation 27
4.1 Introduction 27
4.2 Coventorware Simulation Setup 29
4.3 Simulation Results 33
4.4 Discussion and Comparison 37
4.5 Circuit vs. Mechanical Analysis 38
4.6 Conclusion 41
Chapter 5 Fabrication Measurement Results 42
5.1 Introduction 42
5.2 Measurement Results 42
5.3 Quality Factor 48
5.4 Observations 48

5.4.1 Post-process 50
5.5 Second Run 52
Chapter 6 Conclusions 59
6.1 Contributions 59
Bibliography 60

List of Figures

Figure 2.1 Typical SAW configuration [5] 3
Figure 2.2 One-port SAW [6] 4
Figure 2.3 Rectangular-shaped SAW resonator [10] 5
Figure 2.4 Ring-shaped SAW resonator [10] 6
Figure 2.5 Displacement of IDTs at resonance frequencies [11] 7
Figure 2.6 SAW resonator response [11] 8
Figure 2.7 SAW resonator with reflectors [12] 8
Figure 2.8 BVD model for SAW 9
Figure 2.9 Typical SAW response with f_r and f_{ar} 9
Figure 2.10 Acoustic wave resonator using AlN [14] 10
Figure 2.11 Two-dimensional AlN resonator [18] 11
Figure 2.12 LFE CLMR [19] 11
Figure 2.13 High Q low-resistance AlN resonator [20] 12
Figure 2.14 FEM-based analysis of GaN SAW in COMSOL [22] 14
Figure 2.15 FEM-based analysis in COMSOL [12] 14
Figure 2.16 Ansys simulation of SAW resonator [23] 15
Figure 2.17 SAW resonator with additional series capacitance 16
Figure 2.18 SAW resonator with additional parallel capacitance 16
Figure 2.19 Resonator using three series and two shunt resonators [25] 16
Figure 2.20 Shunt inductance to create acoustic wave lumped element resonator (AWLR) 17
Figure 2.21 Adding shunt inductance response [26] 18
Figure 2.22 Adding port impedances to change BW [27] 19
Figure 3.1 Cross-section of PiezoMUMPs fabrication (not to scale) 20
Figure 3.2 PSG (purple) deposited on SOI, which is also protected by bottom oxide 22
Figure 3.3 Thermal oxide is grown and patterned by the first mask, PADOXIDE 22
Figure 3.4 Piezoelectric material is deposited by reactive sputtering and patterned using positive photoresist and the second mask, PZFILM 23
Figure 3.5 The metal is deposited via negative photoresist and the third mask, PADMETAL 23
Figure 3.6 The top silicon can be etched to create via holes with DRIE and SOI mask level 24
Figure 3.7 Polyimide coating to protect top layers 24

Figure 3.8 Silicon in the handle layer is etched from the bottom with the mask TRENCH, after which the oxide is etched using chemical wet etch 25
Figure 3.9 The front side protection is removed and the fabrication process is done 25
Figure 4.1 Surface acoustic wave resonator dimensions 28
Figure 4.2 COMSOL simulated model of SAW resonator with 6 fingers 28
Figure 4.3 Process used for Coventorware simulation 29
Figure 4.4 Simple layout for 6-finger resonator (AlN, Metal, SOIHOLE) 30
Figure 4.5 Mesh setting for the simulation 31
Figure 4.6 Meshed structure 31
Figure 4.7 Analysis setup for the simulation 32
Figure 4.8 Admittance for 6-finger resonator 33
Figure 4.9 Admittance of 12-finger resonator 34
Figure 4.10 Admittance for 18-finger resonator 35
Figure 4.11 Twelve-finger resonator with reflector 36
Figure 4.12 Eighteen-finger resonator with reflectors 37
Figure 4.13 Mechanical vs. circuit components 39
Figure 4.14 Designed filter 40
Figure 4.15 Circuit model for the mechanical filter 40
Figure 4.16 S11 of mechanical filter acquired by ADS 41
Figure 5.1 SEM image of 94-finger resonator 42
Figure 5.2 S11 (log magnitude) of the 94-finger resonator 43
Figure 5.3 Phase of S11 in degrees showing the biggest change around the main resonance frequency 44
Figure 5.4 S11 on the Smith chart, with each circle corresponding to a certain resonance frequency and the biggest circle being the main resonance 45
Figure 5.5 S11 dB 46
Figure 5.6 S11 phase 46
Figure 5.7 BVD circuit model for 94-finger resonator 47
Figure 5.8 S11 (dB) Simulation and fabrication, with the right side being the simulation result of S11, and left side the fabrication result 47
Figure 5.9 The designed layout of different resonators and filter sent to MEMSCAP 49
Figure 5.10 50 Ohm 200-finger resonator without TRENCH 50

Figure 5.11 Ablated structure 51
Figure 5.12 S11 (dB) of the 200-finger 50 Ohm resonator 51
Figure 5.13 Layout sent for fabrication 52
Figure 5.14 Resonator response with 94 fingers 54
Figure 5.15 Resonator with 94 fingers and reflectors 55
Figure 5.16 Resonator with 260 fingers 56
Figure 5.17 Resonator with 307 fingers 57
Figure 5.18 The filter return loss 58
Figure 5.19 Filter insertion loss 58

List of Tables

Table 2.1 Properties of different piezoelectric materials [4] 3
Table 3.1 PiezoMUMPs Layer Colors 22
Table 3.2 Summary of PiezoMUMPs Layers and Their Properties 26
Table 5.1 Three Resonators and Comparison Between the Q-Factors 48

Chapter 1
Introduction

1.1 Motivation

Microwave filters play an important role in telecommunications and satellite systems. Among the many types of microwave filters, acoustic Microelectromechanical Systems (MEMS) filters have received increased attention recently for their simplicity, low cost and higher quality factor.

The three different types of acoustic piezoelectric MEMS filters are bulk, thin film and surface acoustic wave filters. Each of these filters has its own specific properties and fabrication processes, but they all work by converting acoustic vibration to electrical signals, and vice versa. These filters tend to have higher quality factors in frequencies of several hundreds of MHz.

In this research, a new PiezoMUMPs process which was introduced by MEMSCAP in 2013 is used in the fabrication of SAW resonators and filters. The piezoelectric material in this process is aluminum nitride, which is considered able to reach higher quality factors than conventional piezoelectric materials used in SAW, like lithium niobate.

1.2 Objectives

The objective of this research is to explore the theory behind the applications of acoustic filters and mathematical and simulation analysis of the structures. The major research tasks include:

- Analyses and simulation of SAW resonators
- Investigation of the feasibility of using the PiezoMUMPs process in the realizations of SAW resonators and filters.
- Design, fabrication and test of aluminum nitride-based SAW resonators.

1.3 Thesis Outline

Chapter 2 presents a literature review on acoustic filters and resonators in general, along with their applications. Chapter 3 presents the PiezoMUMPs fabrication process in detail, while Chapter 4 talks about the mathematical and simulation analysis of piezoelectric devices and the design procedure of this study. Finally, Chapter 5 provides the measurement and fabrication results, and discusses comparisons between measurements and simulations.

Chapter 2
Literature Review

2.1 Introduction

Microwave filters are important parts of communication systems. Although significant advances have been made in developing new ways to make microwave filters, there is always room for further improvements in the area.

One type of these filters that has attracted more attention recently is the Microelectromechanical Systems (MEMS) filter. MEMS filters usually have higher quality factors, as they incorporate a piezoelectric material. There are several different types of configurations of MEMS filters, including Bulk Acoustic Wave (BAW), Film Bulk Acoustic Resonator (FBAR), and Surface Acoustic Wave (SAW) filters. Each of these filters has its own specifications and fabrication processes. In BAW structures, a layer of piezoelectric material is sandwiched between two layers of metal [1]. This excites the piezoelectric material in bulk mode. An FBAR is the same as BAW, with the only difference being that piezoelectric is used as thin films and has increased frequency of operation, which can function up to a few GHz frequencies [2]. SAW filters, on the other hand, have a different fabrication process. In surface acoustic wave resonators, the surface of the piezoelectric is excited, since there is no metal layer on the bottom of the piezo material [3].

In designing piezoelectric resonators, choosing the right piezoelectric material is an important part of the process. Different piezoelectric materials have different electromechanical properties which could cause different effects on resonance frequency, electromechanical coupling, the fabrication process, etc. There are various kinds of piezoelectric materials, such as zinc oxide, lithium niobate, and aluminum nitride. A comparison of the different properties of these materials can be found in [4].

According to Table 2.1, a piezoelectric material can be selected depending on the specific resonator requirements for a particular application. In this study, we chose aluminum nitride (AlN), in accordance with the PiezoMUMPs® fabrication process.

Table 2.1 Properties of different piezoelectric materials [4]

Materials	ZnO	AlN	$LiNBO_3$	Units
Density	5680	3260	4700	kg/m^3
Longitudinal Acoustic Wave velocity	~6350	~11270	~6550	m/s
Shear Acoustic Wave Velocity	~2720	~6000	~3590	m/s
Piezoelectric Coefficient, e_{33}	1.32	1.55	1.77	C/m^2

2.2 Surface Acoustic Wave Resonators

SAW devices can operate up to a few GHz and can be easily fabricated using conventional MEMS fabrication techniques [5]. In order to create surface waves on a piezoelectric material, the metal electrode on top of the piezoelectric is deposited and then etched to make interdigitated fingers (IDT). As can be seen in Figure 2.1, IDTs can be used as the input and output electrodes for a 2-port network.

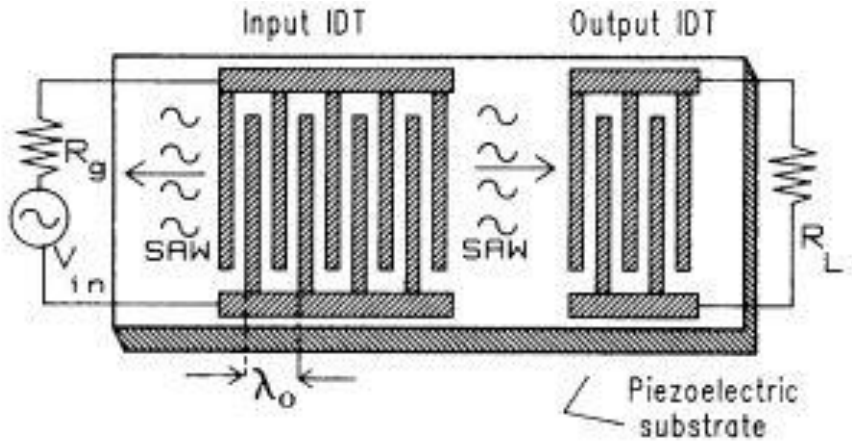

Figure 2.1 Typical SAW configuration [5]

A SAW resonator can be measured either as a 1-port or 2-port device. The designer can choose either one, depending on the measurement facilities to which they have access. Figure 2.2 shows the 1-port resonator in [6].

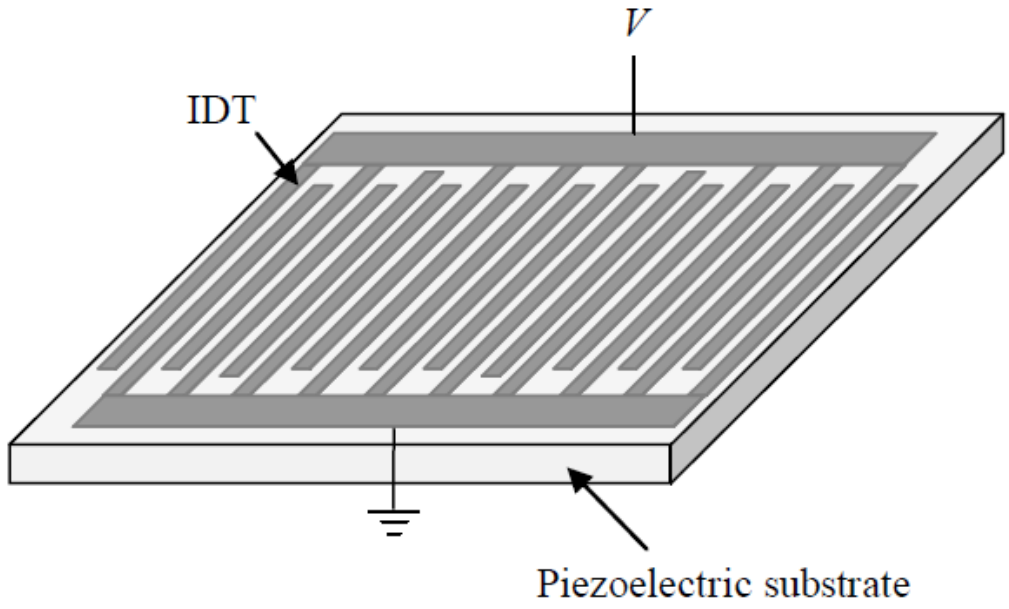

Figure 2.2 One-port SAW [6]

Important features of any SAW structure are its center frequency and the relation between the center frequency with the dimensions of the IDTs and the piezoelectric material properties. As a general rule of thumb, if the acoustic velocity in the piezoelectric material is V and the wavelength is λ, the resonance frequency can be defined by Equation 2.1.

$$\boldsymbol{f = V/\lambda} \qquad \textbf{2.1}$$

Another important physical property of the SAW device is the period of the IDTs, which is defined as the distance between the middle of two adjacent IDTs (one input and one ground). The periodicity (p) is half the wavelength, which means:

$$p = \frac{\lambda}{2}.$$

SAW devices have many practical applications. They have been used as strain sensors [7], microwave filters [8] and in chemical sensing [9]. Surface acoustic wave resonators can also take different shapes, such as rectangular or ring, as can be seen in Figure 2.3 and Figure 2.4 [10].

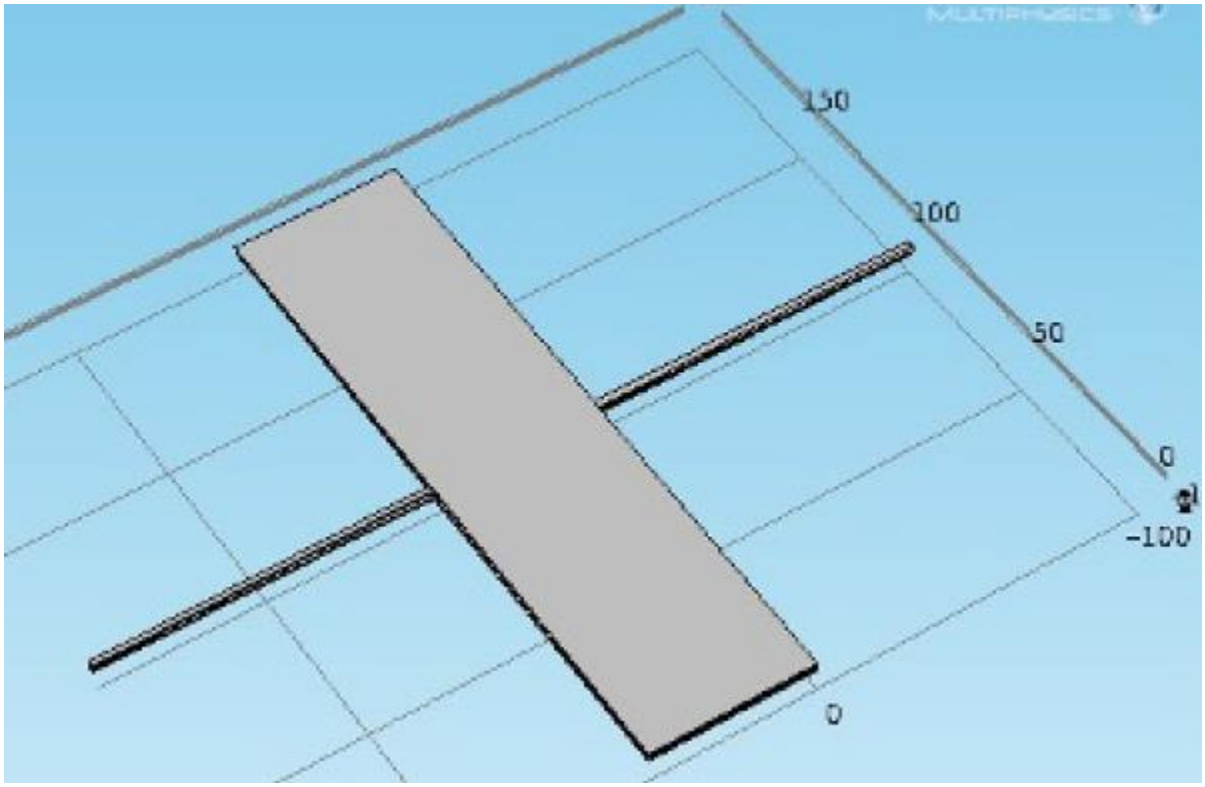

Figure 2.3 Rectangular-shaped SAW resonator [10]

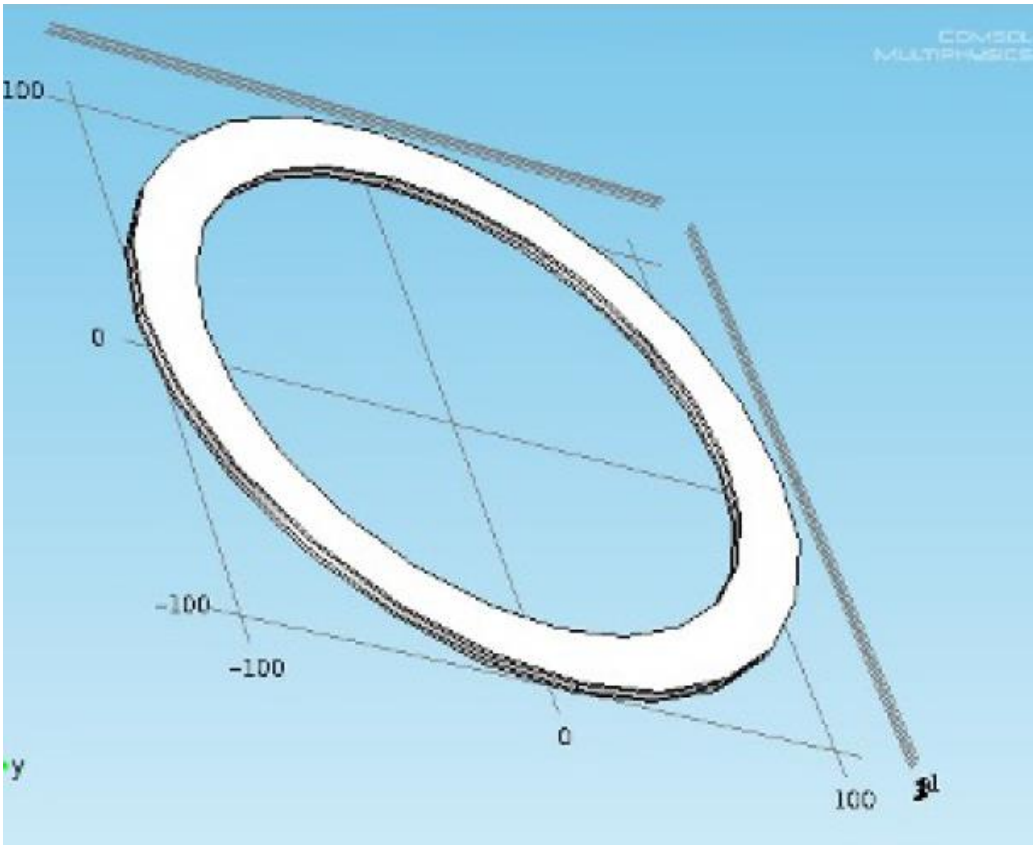

Figure 2.4 Ring-shaped SAW resonator [10]

Surface acoustic wave resonators, like any other resonator, have an infinite number of resonant frequencies. However, the design frequency has the greatest displacement in impedance, admittance or S11 compared to other resonant modes. Displacement refers to the change in magnitude of the characteristics of a SAW resonator such as impedance. By knowing at what frequency the greatest displacement occurs, we can know the device's resonance frequency and can configure an operating point for the resonator.

Figure 2.6 shows an example of the response (susceptance) from a typical surface acoustic wave resonator [11]. As can be seen, the susceptance has the greatest spike at the main resonance frequency. If we look at the displacement of the IDTs, we can see a huge spike at the main resonance frequency in contrast to other resonances (Figure 2.5). Another aspect that is usually considered in SAW resonators is utilizing two sets of reflectors on two sides of the IDTs. Reflectors are IDTs that have the same periodicity as IDTs but are not connected to either signal or ground and are placed on

top of the piezoelectric material. The reflectors capture the acoustic energy and reflect it back to the IDTs so that the dissipation of energy is smaller and the quality factor thus becomes larger [12].

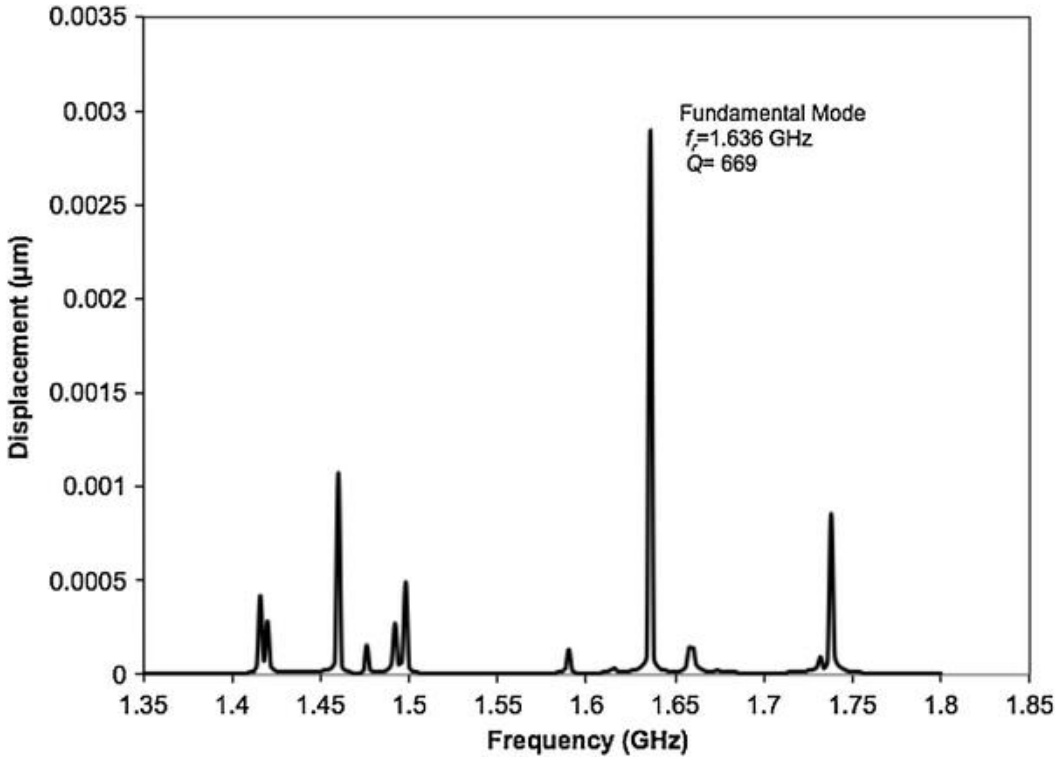

Figure 2.5 Displacement of IDTs at resonance frequencies [11]

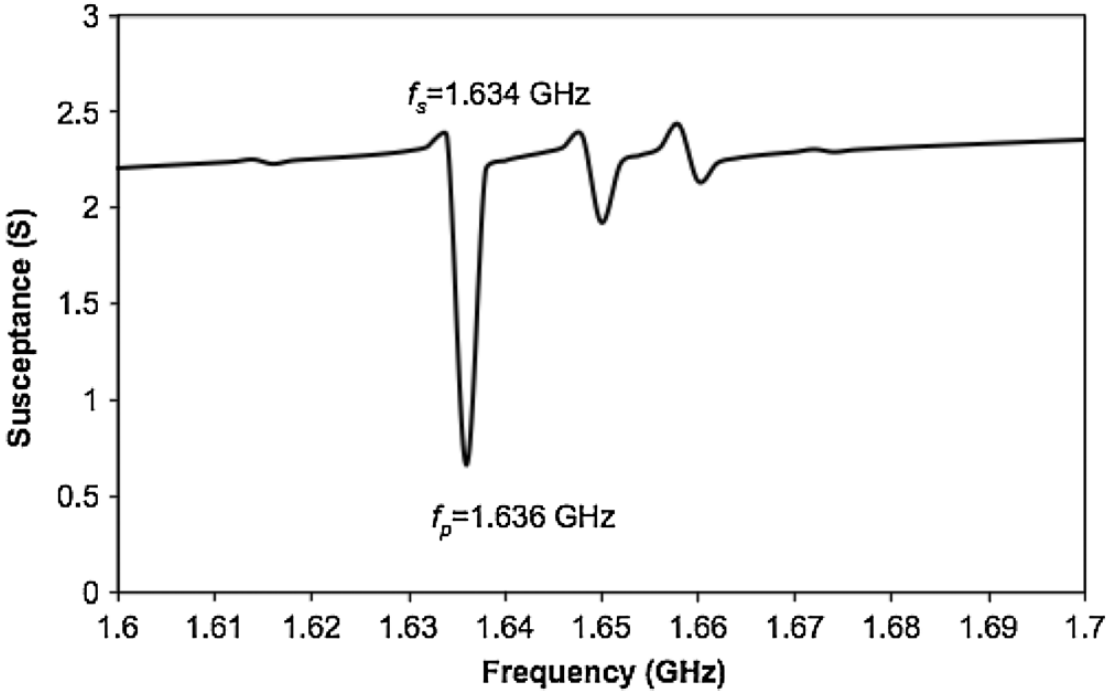

Figure 2.6 SAW resonator response [11]

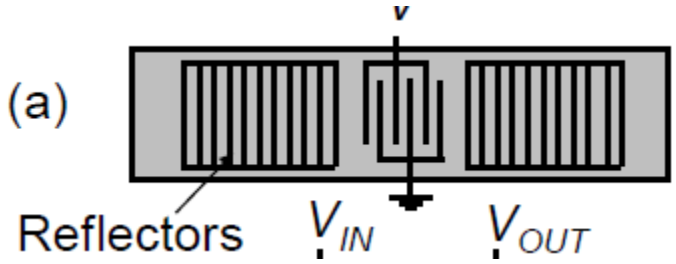

Figure 2.7 SAW resonator with reflectors [12]

In order to analyze the SAW resonators, an equivalent electrical circuit needs to be extracted. A SAW resonator consists of four lumped elements: motional inductance (L_m), motional capacitance (C_m), motional resistance (R_m) and static capacitance (C_0) [13]. Figure 2.8 shows the Butterworth Van Dyke (BVD) model, which represents not only SAW but any acoustic resonator around its fundamental resonance frequencies. To formulate these components in terms of the physical characteristics of SAW, we have to take a closer look at the resonance frequency of the SAW resonator response. As depicted in Figure 2.9, there are two spikes in impedance (or admittance) at resonance frequencies. One is called resonance frequency (f_r), and the other is called anti-resonance

frequency (f_{ar}). Resonance frequency is also called series resonance, and anti-resonance is also called parallel resonance.

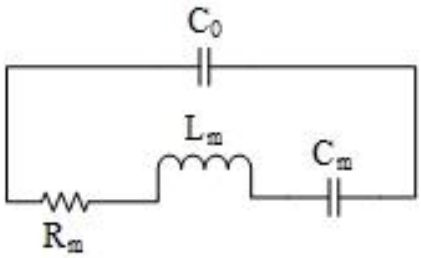

Figure 2.8 BVD model for SAW

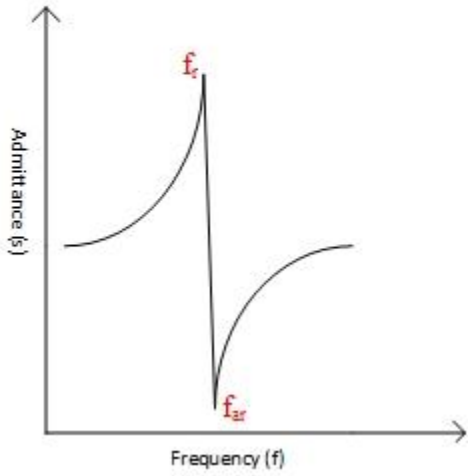

Figure 2.9 Typical SAW response with f_r and f_{ar}

According to these figures, we can formulate the lumped components as the following equations [4]:

$$f_r = \frac{\omega_r}{2\pi} = \frac{1}{2\pi}\sqrt{\frac{1}{L_m C_m}} \quad 2.2 \quad [4]$$

$$f_{ar} = \frac{\omega_{ar}}{2\pi} = f_r\sqrt{1+\frac{C_m}{C_0}} \quad 2.3 \quad [4]$$

$$Q_r = \frac{1}{\omega_r R_m C_m} \quad 2.4 \quad [4]$$

$$Q_{ar} = \frac{1}{\omega_{ar} R_m C_m} \qquad 2.5 \quad [4]$$

where Q_r and Q_{ar} are loaded Q-factors at f_r and f_{ar}, respectively. From Equation 2.1, we know that the series resonance or f_r is equal to the ratio of acoustic velocity by the wavelength. So, we can design the series frequency and find the static capacitance by simulation or mathematical analysis. After measuring the resonator response, we can then find the rest of the lumped element components.

2.3 Aluminum Nitride SAW Resonator

As mentioned in section 2.1, various piezoelectric materials can be used in acoustic wave resonators. Aluminum nitride has received increased attention recently with the introduction of PiezoMUMPs fabrication rules by MEMSCAP™ in 2013. Several papers in the literature utilize AlN as their piezoelectric for acoustic wave devices [14], [15], [16], [17].

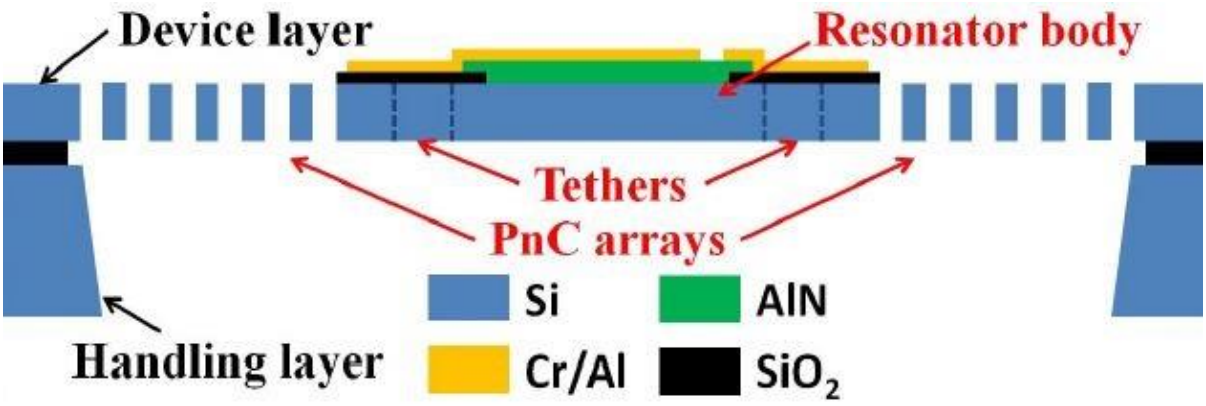

Figure 2.10 Acoustic wave resonator using AlN [14]

Another example of a device which uses AlN is a 2-dimensional mode resonator like [18]. In that paper, there is only one set of IDTs and this is used only for the signal electrode, as shown in Figure 2.11.

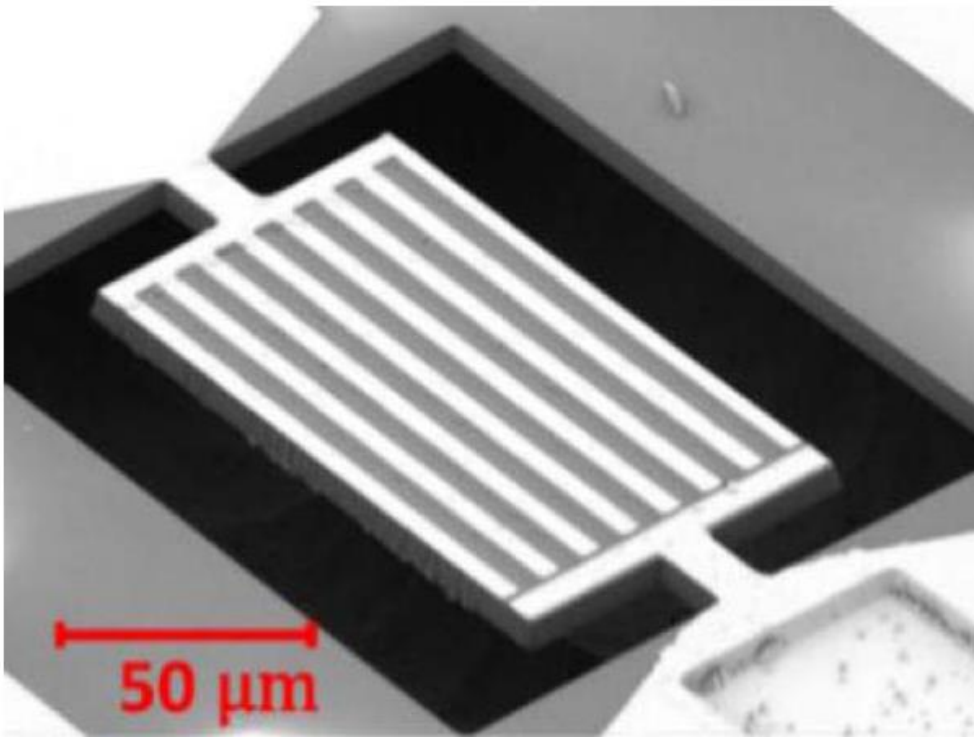

Figure 2.11 Two-dimensional AlN resonator [18]

Another configuration in the literature that uses AlN is the cross-sectional lame mode resonator (CLMR), which is used in two structures. One of them utilizes bottom electrodes (fBAR), while the other, which is called lateral field excitation or LFE, has no bottom IDT (SAW). The frequency of operation is around 1 GHz and 2.8 GHz and there is an increase in k_t^2 [19].

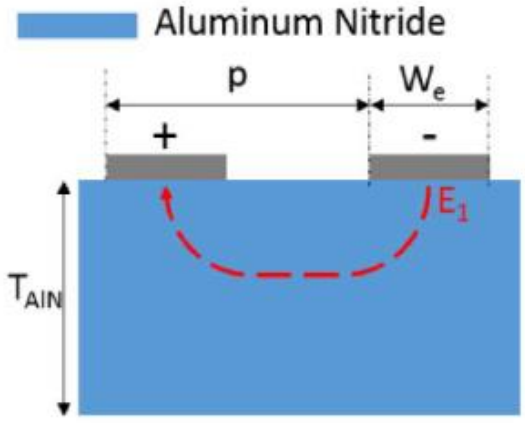

Figure 2.12 LFE CLMR [19]

In another study, quasi-symmetrical lamb waves were used to achieve high quality (Q>10000) and low motional impedance (R_m<50 Ω). In the study, AlN on an Si wafer was used as the structural layer, and the frequency of operation was 260 MHz [20].

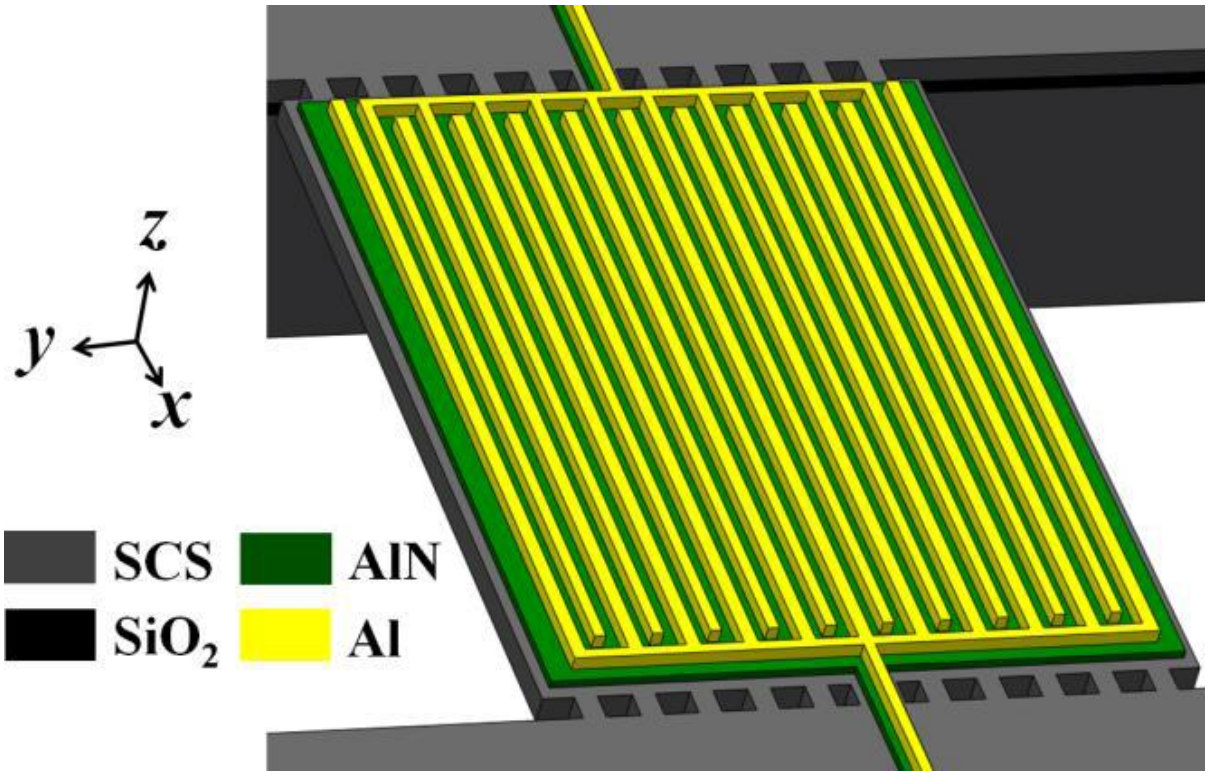

Figure 2.13 High Q low-resistance AlN resonator [20]

Many other configurations and applications can be used for designing AlN SAW resonators, but these are beyond the scope of this research.

2.4 Finite Element Analysis of SAW

Finding the anticipated response from the MEMS devices can be done in several ways, including lumped element (ad hoc), mathematical analysis, and finite element analysis (FEA). Each of these approaches has advantages and disadvantages. The lumped element technique can give us a good idea of the device response, but only in a narrow frequency range, since lumped elements cannot contain all of the mechanical properties of the SAW devices. Mathematical models can be helpful, but as the device becomes larger and more complex, the number of equations likewise grows, making it very difficult and time-consuming. The finite element approach can be extremely useful for MEMS structures. In this method, the structure is reduced to very small meshes and the differential equations

governing the structure are solved in each mesh. If the results converge with an acceptable error, the analysis returns an answer [21].

The biggest advantage of the finite element method is that the device can be simulated in three dimensions, so the designer can get a good idea of the actual device response. Several different software programs, such as COMSOL, Ansys and Coventorware, can be used to do a finite element analysis on MEMS devices. These software programs are commercially available and widely used in MEMS design and fabrication.

Although simulating in 3-D is the biggest advantage of FEM-based software, the results can also be unreliable depending on the choice of mesh size. In FEM-based software, the bigger the mesh size, the more unreliable the result is. When the mesh becomes smaller in a 3-D structure, there is an exponential increase in simulation time. So, there is a trade-off between accuracy and simulation time.

In SAW structures, since the IDTs are periodic, the structure can be reduced to a smaller size and periodic boundary conditions can be defined. This reduces the size of the structure and thus reduces the simulation time. In addition, since the thickness of the piezoelectric material and the periodicity of the IDTs (and not their length) play the most important role in SAW responses, we can simulate the 2-D structure instead of a 3-D one, which reduces the simulation time by a significant factor. Figure 2.14 and Figure 2.15 are examples of 2-D simulations in the literature.

An important feature of FEM software is that material properties are predefined and editable, so the designer can use them for characterization [22]. Furthermore, the BVD model can be extracted from the response of the FEM software [12]. In addition to COMSOL, ANSYS can be used to simulate the MEMS structures to find the response of the SAW structure [23], as can be seen in Figure 2.16. In this work, zinc oxide was used [23].

Almost all of the simulations in the literature were done in 2-D instead of 3-D, and the simulation and measurement results match perfectly. In this study, both COMSOL and Coventorware are used and the detailed procedure is outlined in the simulation section.

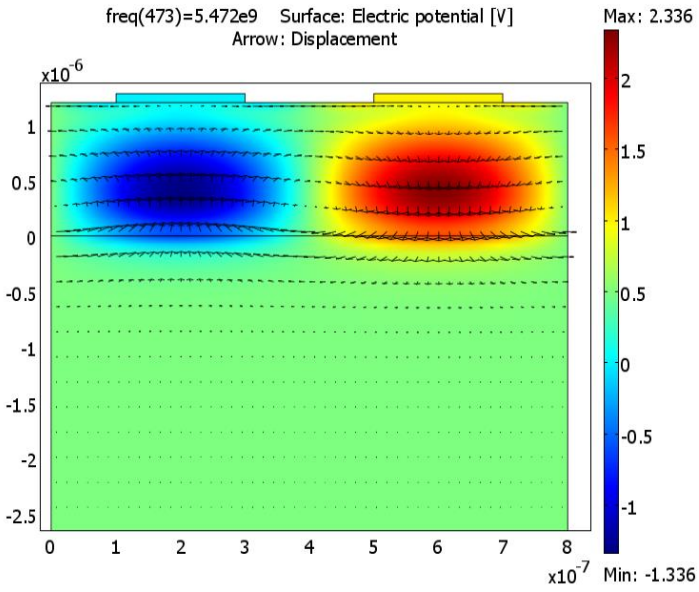

Figure 2.14 FEM-based analysis of GaN SAW in COMSOL [22]

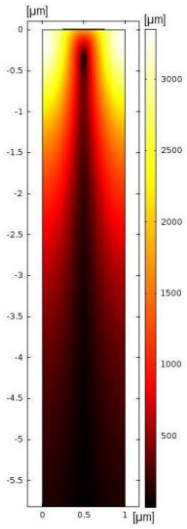

Figure 2.15 FEM-based analysis in COMSOL [12]

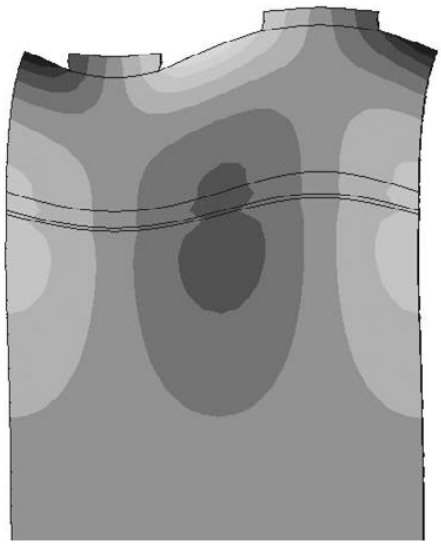

Figure 2.16 Ansys simulation of SAW resonator [23]

2.5 Tunable SAW Filter

Numerous attempts have been made in the literature to develop acoustic tunable filters. Some of these efforts were more successful than others [24]. The idea behind tunable filters is to change the bandwidth or center frequency of the filter by tuning the resonators of the filter. Since each resonator has a BVD model, the tuning can be done on the circuit level and then reverse-engineered to physical dimensions. Usually by adding a capacitor in series or parallel to the resonator, one can tune the f_r or f_{ar} of the resonator, depending on the parallel or series connection of the additional capacitor. From Equations 2.2 and 2.3, we know the formula to find resonance and anti-resonance frequencies from lumped components or vice versa. When an additional capacitance is connected in series (parallel) to the resonator, the f_r (f_{ar}) will be changed using Equations 2.6 and 2.7.

$$f'_r = f_r\sqrt{1+\frac{C_m}{C_0+C_s}} \qquad \textbf{2.6}$$

$$f'_a = f_r\sqrt{1+\frac{C_m}{C_0+C_p}} \qquad \textbf{2.7}$$

where C_s and C_p are the series and parallel additional capacitors, respectively.

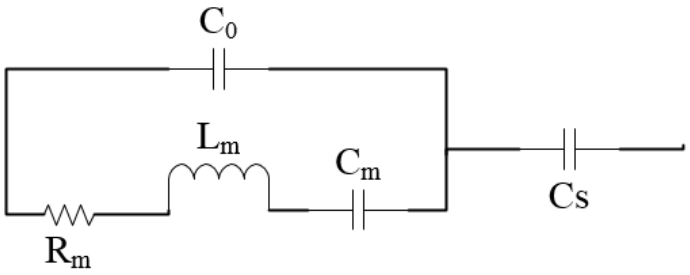

Figure 2.17 SAW resonator with additional series capacitance

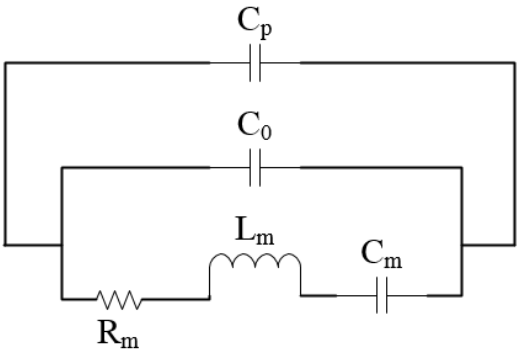

Figure 2.18 SAW resonator with additional parallel capacitance

For example, if a filter consists of three series and two shunt resonators, as in Figure 2.19, series and parallel capacitors can be added to make the filter tunable [25]. By changing the additional capacitances, the bandwidth (BW) can also be changed.

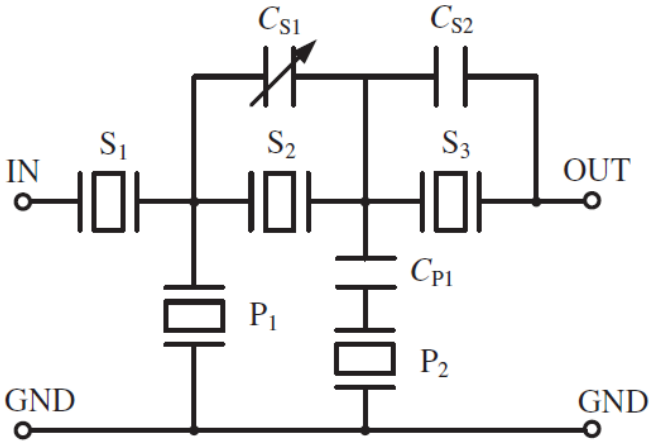

Figure 2.19 Resonator using three series and two shunt resonators [25]

Another example of making SAW resonators somewhat tunable is to move f_{ar} away from f_r and use f_r as a bandstop filter, since the response at the resonance frequency is very high quality. These filters are called acoustic wave resonator based filters [26]. To do this, a shunt inductor is added to the SAW resonator to move the anti-resonance frequency, as shown in Figure 2.20. In Figure 2.21, the added inductance L_p shifted f_{ar}, from f_r, and created a bandstop filter using only the resonance frequency.

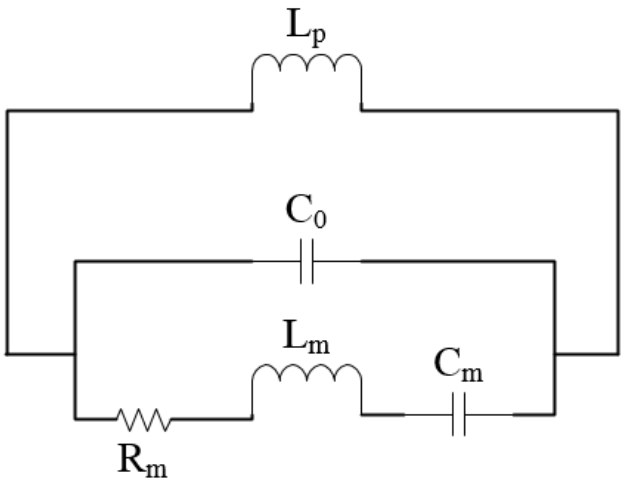

Figure 2.20 Shunt inductance to create acoustic wave lumped element resonator (AWLR)

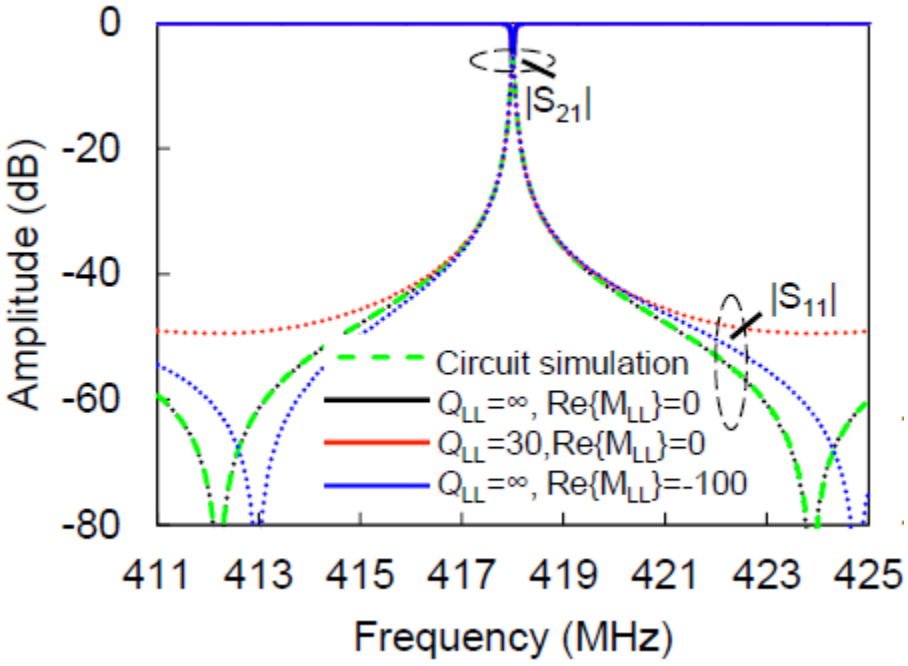

Figure 2.21 Adding shunt inductance response [26]

To find the appropriate value for L_p, we have to figure out what happens to the resonance frequency mathematically. The important point to consider here is that we need to adjust the anti-resonance and not the resonance [27]. The idea is to remove the effect of C_0 on the f_{ar} by adding an inductor parallel to it that produces a resonance at f_r.

$$\boldsymbol{L_p = \frac{1}{4\pi^2 f_r^2 C_0}} \quad \textbf{2.8}$$

After calculating the desired value, we can add it to the resonator and make whatever tunability we want. Adding 90^o transmission lines can be effective for changing the BW of resonance at f_r. The bandwith can also be changed by using different port impedances than the input impedance of the resonator (Z_o), which we assume as 50 Ω.

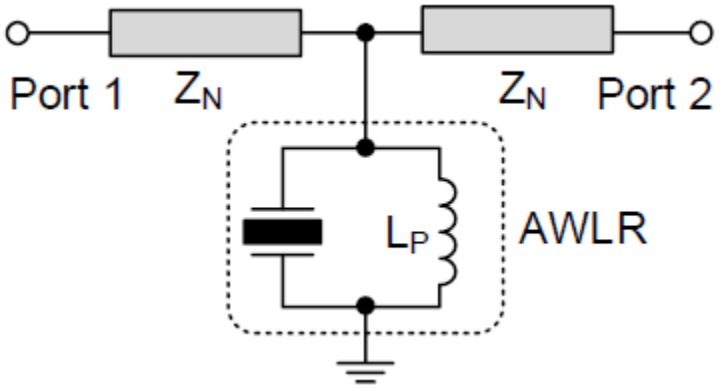

Figure 2.22 Adding port impedances to change BW [27]

$$r = \left(\frac{Z_n}{Z_o}\right)^2 \qquad \textbf{2.9}$$

$$BW_{AWLR} = rBW_{res} \qquad \textbf{2.10}$$

As mentioned previously, there are many different ways to create tunable acoustic filters. According to the application and fabrication processes, any of these techniques can be used.

Chapter 3
PiezoMUMPs Process

3.1 Introduction

In this study the PiezoMUMPs fabrication by MEMSCAP™ is used for fabricating the SAW resonators. MEMSCAP provides three other different Multi-User MEMS Processes or MUMPs®: MetalMUMPs, PolyMUMPs and SOIMUMPs. The PiezoMUMPs is an addendum to SOIMUMPs that can be used for fabricating various fabrications featuring piezoelectric materials such as acoustic devices [28]. A cross-section of the fabrication layers for PiezoMUMPs can be seen in Figure 3.1.

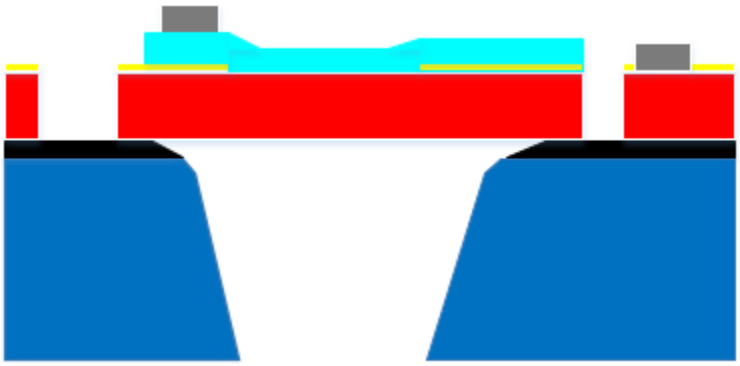

Figure 3.1 Cross-section of PiezoMUMPs fabrication (not to scale)

A summary of the PiezoMUMPs is described below (the detailed fabrication steps are given in section 3.2):

1. The SOI wafer used as the substrate is <100> oriented. It uses 400 μm thick silicon as a handle layer, along with 1 μm of oxide and 10 μm of silicon on top of the oxide.
2. The top silicon can be etched down to the oxide to make vias or mechanical figures. The top silicon is doped first.
3. The 400 μm substrate can be etched from the bottom and stop at the oxide layer. This layer can make holes that can be used as through points.
4. A thermal oxide layer can be patterned on top of the silicon to create electrical isolation between the silicon and metal layers.

5. The piezoelectric layer, which is the AlN, creates the piezoelectricity needed for acoustic wave devices.
6. The metal layer is patterned on top of the silicon to create electrodes.

3.2 Fabrication Process

In PiezoMUMPs, only five masks are used. The fabrication process is described in detail in this section. As mentioned previously, the AlN used in the PiezoMUMPs process has a d_{33} of 3.4-6.5 pC/N, with d_{33} being the piezoelectric strain coefficient. As mentioned in section 3.1, an n-type <100> oriented silicon on insulator starts the process. A layer of phosphosilicate glass is deposited on top of the silicon and it is annealed at $1{,}050^{o}$ in Argon to dope it. The PSG layer is removed afterwards, using chemical wet etch. The first mask to be used is PADOXIDE, which has a thickness of 2000 Å. This layer is not deposited but grown and patterned using RIE, and is the layer that can be used to make electrical insulation.

So, the first deposited layer is the Aluminum Nitride or AlN. It has a thickness of 500 nm and is defined by a PZFILM mask. AlN is patterned by wet etch.

After the piezoelectric material, the second deposited layer is aluminum. Since aluminum will not stick to the layers below, there should be some kind of adhesion. In this case, the adhesion is chromium, so 20 nm of chromium is used. For creating switches where the aluminum is used for electrical connections, the thickness of the metal is $1\mu m$, but for acoustic applications, as given by MEMSCAP, the thickness of PADMETAL is 520 nm. The silicon etching is done using the SOI mask level. The special recipe of SOI from MEMSCAP prevents the undercutting of the silicon.

The last mask, TRENCH, is used to etch the silicon from the bottom. First, a protective layer is used for the top parts and RIE does the bottom etch. Then, to remove the buried oxide, a wet etch follows the RIE.

The minimum feature size in the PiezoMUMPs process is 2 μm [29].

Table 3.1 shows the colors used for each layer in the graphs.

Silicon	Substrate	Bottom Oxide	Pad Metal
Buried Oxide	Piezoelectric Material	Pad Oxide	Front Side Protection

Table 3.1 PiezoMUMPs Layer Colors

Figure 3.2 PSG (purple) deposited on SOI, which is also protected by bottom oxide

Figure 3.3 Thermal oxide is grown and patterned by the first mask, PADOXIDE

Figure 3.4 Piezoelectric material is deposited by reactive sputtering and patterned using positive photoresist and the second mask, PZFILM

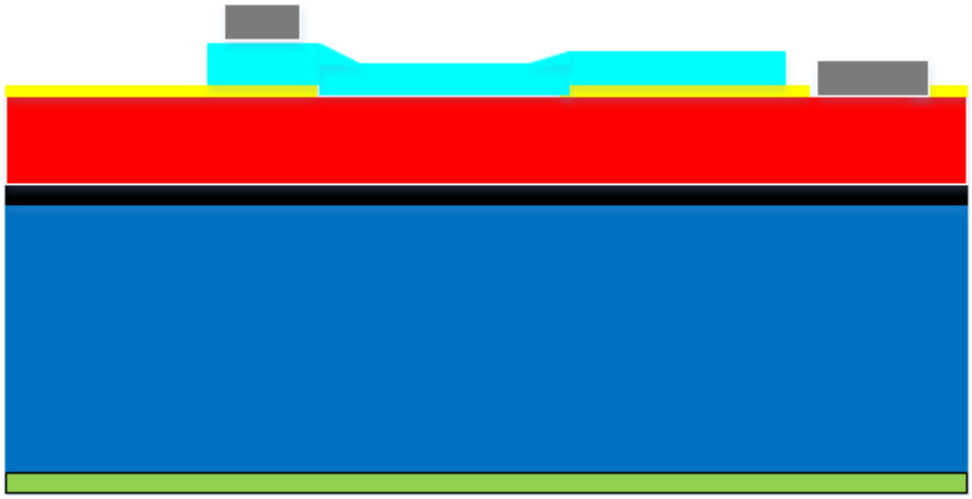

Figure 3.5 The metal is deposited via negative photoresist and the third mask, PADMETAL

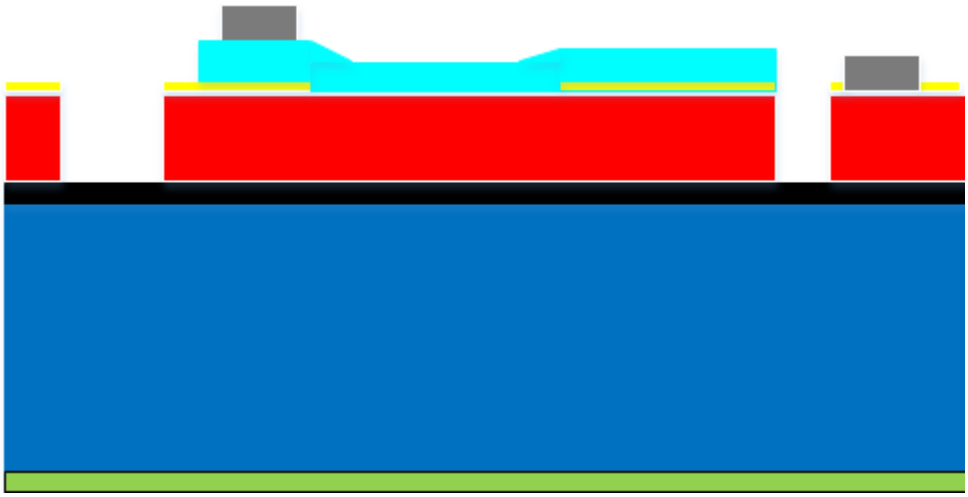

Figure 3.6 The top silicon can be etched to create via holes with DRIE and SOI mask level

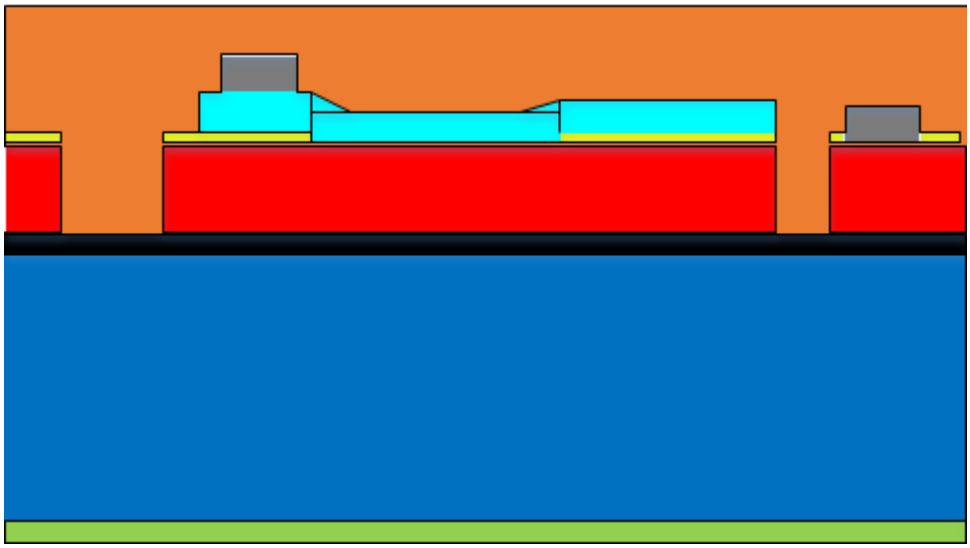

Figure 3.7 Polyimide coating to protect top layers

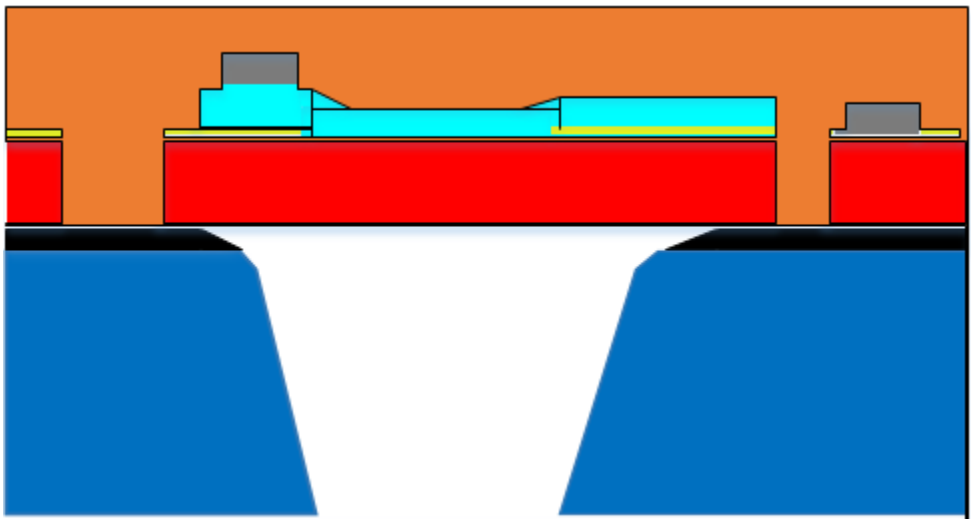

Figure 3.8 Silicon in the handle layer is etched from the bottom with the mask TRENCH, after which the oxide is etched using chemical wet etch

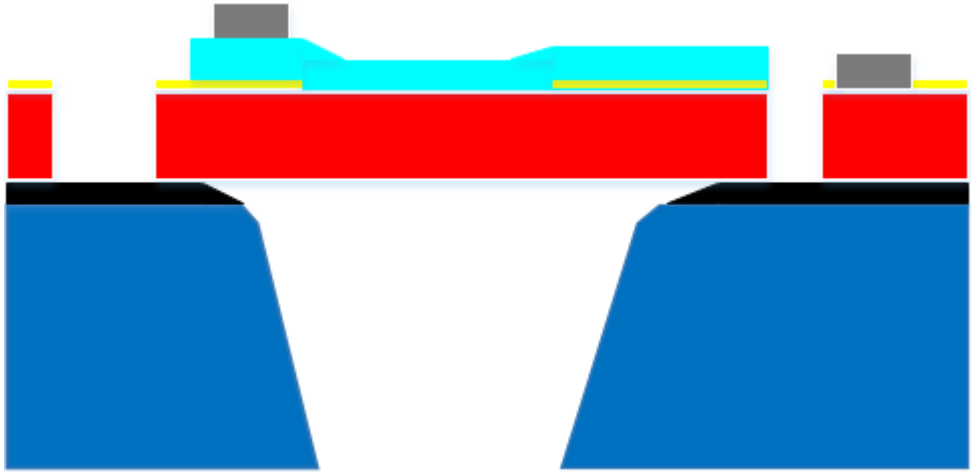

Figure 3.9 The front side protection is removed and the fabrication process is done

A summary of the levels, masks, thicknesses, and minimum sizes of each layer can be seen in Table 3.2.

Table 3.2 Summary of PiezoMUMPs Layers and Their Properties

Material	Thickness (μm)	Mask Level Name	Minimum Feature (μm)
Pad oxide	0.2	PADOXIDE	5
Piezoelectric Material	0.5	PZFILM	10
Pad Metal	0.52	PADMETAL	3
Silicon	10	SOI	2
Oxide	1	N/A	N/A
Substrate	400	TRENCH	200

Chapter 4
Simulation

4.1 Introduction

In this study, finite element analysis is carried out using the commercially available software COMSOL and Coventorware to design SAW resonators. A combination of these two FEM software packages was needed to get the proper results and to create the resonator models. Although both of these software programs have the ability to simulate the MEMS Piezoelectric structures, with the addition of the fastpze add-on to the Coventorware, the simulation of 3-D MEMS Piezoelectric structures becomes almost 30 to 40 times faster than other FEM software packages such as COMSOL. In this chapter, the simulation we used will be discussed in detail.

The design process of the surface acoustic structures starts with choosing a frequency of operation. According to Equation 2.1, the frequency can be related to the acoustic velocity of the piezoelectric material and the wavelength. The wavelength is considered to be twice the periodicity of the fingers. We designed the resonator to operate at 450 MHz; since the acoustic velocity is 10127 m/s [30], the wavelength will be approximately 24 microns (λ). This leads to a 12-micron period (p) and 6-micron electrode width (w), as can be seen in Figure 4.1. Once the device dimensions are calculated, the number of fingers needs to be determined to start the design. A combination of analytical and simulation approaches is used to find the number of fingers., The equivalent circuit of a SAW resonator is the Butterworth-Van-Dyke (BVD) model given in Figure 2.8. The C_0 in this circuit is the static capacitance. To find the number of fingers, the input impedance (Z_0) of the resonator needs to be defined in order to find the static capacitance at that frequency. The defined impedance for one of the resonators, for example, is 106 Ω. Using Equation 4.1, C_0 is calculated to be 3.336 pF.

$$C_0 = \frac{1}{2\pi f Z_0} \qquad \textbf{Equation 4.1}$$

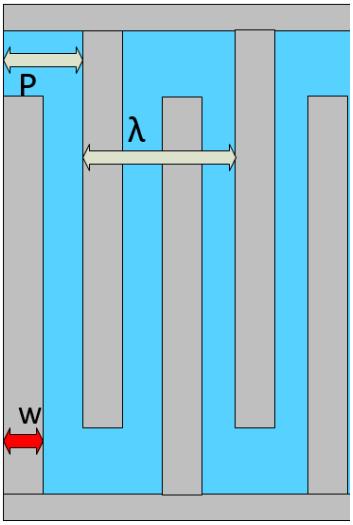

Figure 4.1 Surface acoustic wave resonator dimensions

COMSOL is used as a simulation tool to determine how many fingers can satisfy this capacitance. In COMSOL, there is a built-in function to find out the capacitance of a structure in different conditions or frequencies. A structure with only 6 fingers was simulated in COMSOL, as shown in Figure 4.2 (the air box around the structure to account for the fringing fields is removed to show the fingers more clearly). After the C_0 of 6 fingers is found, we can find the number of fingers needed to realize the required Co value since the addition of IDTs acts effectively as parallel capacitors.

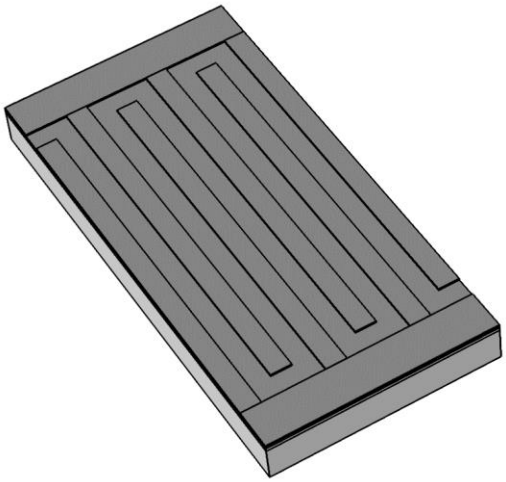

Figure 4.2 COMSOL simulated model of SAW resonator with 6 fingers

The COMSOL simulation for the 6 finger structures yields a capacitance value of 0.213 pF. Therefore, to achieve a capacitance of 3.336 pF, we need 94 fingers. The simulation does not end

here. After calculating the required number of fingers, we have to simulate the whole structure to find out the response of the circuit over a certain frequency range. Simulating 3D structures in COMSOL is a step that takes a huge amount of time and is essentially unfeasible. However, in Coventorware, there is a new Add-On called fastpze that combines python with 3D simulation and gives accurate results much faster than COMSOL. Even though fastpze is fast, simulating the whole structure with small meshes to obtain accurate results still takes a long time and a lot of CPU. With this in mind, structures with 6, 12 and 18 fingers were selected. A meaningful mathematical relationship was then found to approximate the response of the actual structure with 94 fingers. Another advantage of Coventorware is that it provides the BVD model as part of the results. Therefore, by finding the relationship between the BVD components of 6, 12 and 18 fingers the BVD circuit model for the 94 fingers resonator can be approximated.

4.2 Coventorware Simulation Setup

To simulate the structures, the dimensions of the structures need to be listed. The important parts of the dimensions that are under the control of the designer are finger length, width and period, which in this case are 106, 6 and 12 μm, respectively. The simulation is started with 6 fingers, then 12, then 18, and so on. After each simulation, the BVD circuit elements are extracted. The values for C_o, C_m, L_m, and R_m for the different structures are then compared to see if the values match with the mathematical model.

For the purpose of this simulation, the tutorial provided by the Coventor for using the fastpze module was used. The procedure was modified to make it like the PiezoMUMPs process. The first step in Coventorware is defining the process. The defined fabrication process can be seen in Figure 4.3.

0	Substrate	Substrate	SILICON_100	10	LN				
1	Stack Material	LN	AlN	0.5					
2	Stack Material	Metal	ALUMINUM_FILM	0.52					
3	Straight Cut				Metal	+		0	0
4	Straight Cut				ReleaseHoles	-		0	0

Figure 4.3 Process used for Coventorware simulation

As shown in the picture, this is a 2-mask process which has been simplified from the real PiezoMUMPs, since the complexity is not needed for these types of simulations. The next step is drawing the layout. The first layout with 6 um pitch and 6 fingers can be seen below in Figure 4.4.

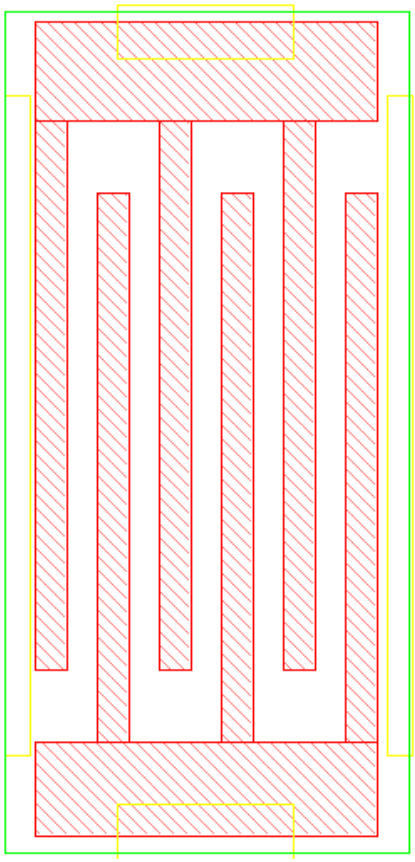

Figure 4.4 Simple layout for 6-finger resonator (AlN, Metal, SOIHOLE)

After the layout is done, the meshing begins. The meshing is performed by using the smart mesh of the Coventor simulator. According to the tutorial, the best mesh to use is Manhattan Bricks. The mesh settings and meshed structure are shown in Figure 4.5 and Figure 4.6, respectively.

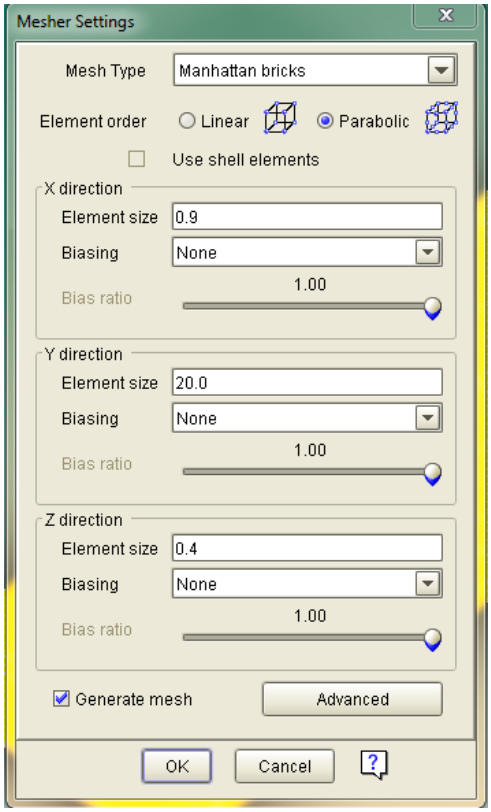

Figure 4.5 Mesh setting for the simulation

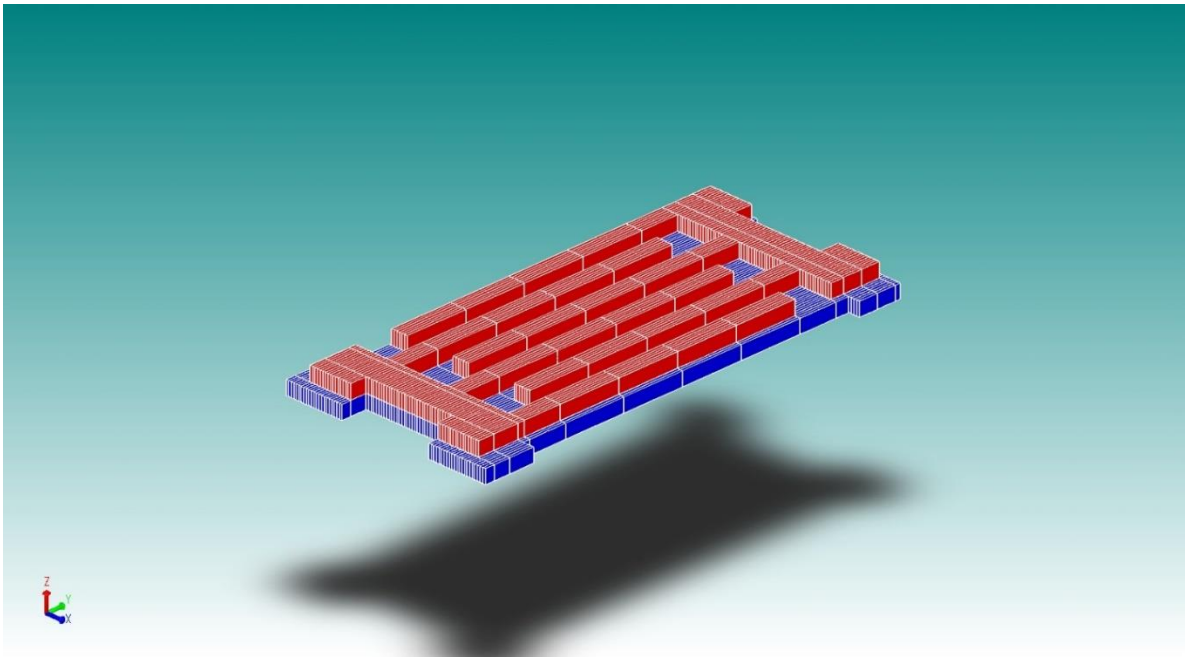

Figure 4.6 Meshed structure

The same mesh settings are used for all the structures made in this work. After meshing, the next step is naming the boundaries so that the boundary conditions on these faces can later be defined. The boundaries are GndEnd, InputEnd, VGnd and Vin. The first two define the fixed boundary conditions, while the second two define the ground and signal, respectively. After defining the faces, the piezoelectric analysis needs to be set up. The analysis is MemMech Piezoelectric analysis, the specifications for which are shown in Figure 4.7. The boundary conditions are defined in this analysis setup. After the setup is done, the script of the analysis is saved and imported in the script part of the Coventorware. Then a Python code is written to use a combination of MemMech and fastpze to expedite the simulation time.

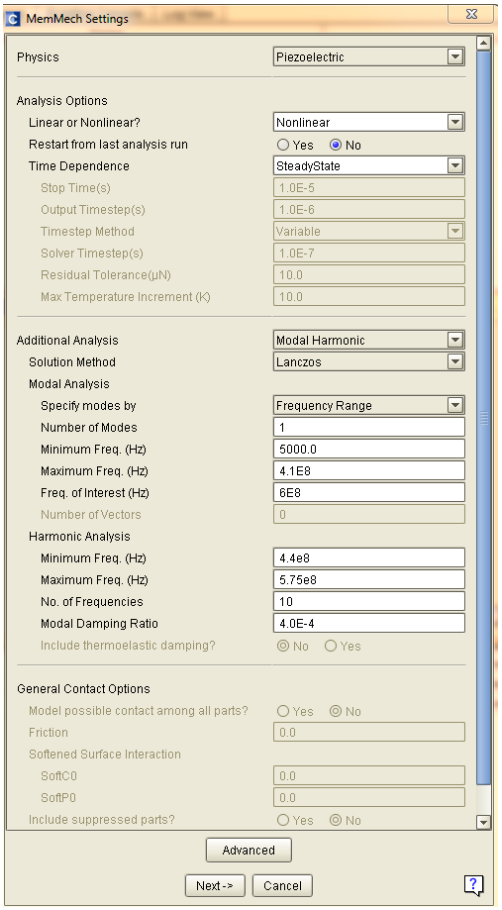

Figure 4.7 Analysis setup for the simulation

The codes are as follows:

```
import fastpze
```

```
modelName = 'PZE_Resonator_prebuilt'

baseScript = 'n_port_Vin.py'

portList = ['Vin']

baseAnalysisName = 'PZEAnalysis1'

a = fastpze.Analyzer(baseScript, portList, baseAnalysisName, modelName)
```

4.3 Simulation Results

After the simulation has been set up, the results are exported from the Coventorware solver. The results of these simulations are reported in this section. First, resonators with 6 um pitch and 6 fingers are chosen. The admittance response vs. frequency (410 MHz to 600 MHz) is depicted in Figure 4.8.

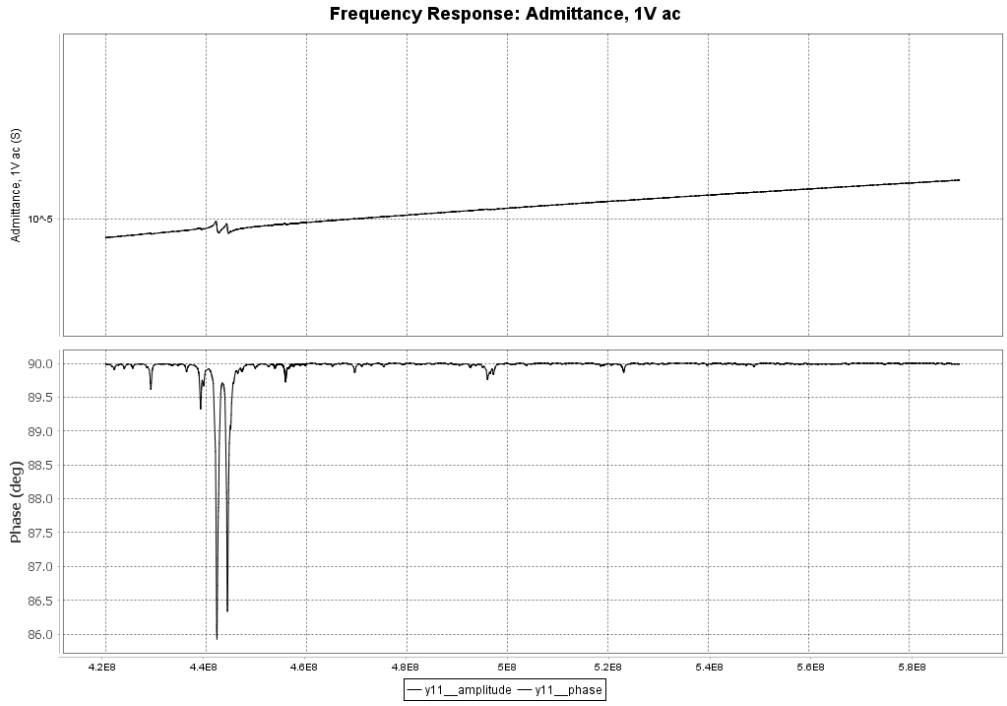

Figure 4.8 Admittance for 6-finger resonator

The next part of the results is the extraction of the BVD model components. You can see the results and also what formulas were used to find out the values of BVD components. The components for the 6-finger resonator are shown below.

Motional resistance, Rm = 1511939.48778 Ohm, Motional inductance, Lm = 0.518522455813 H, Motional capacitance, Cm = 2.49847414664e-19 F, Series resonance frequency, fs = 442179818.488 Hz, Parallel resonance frequency, fp = 442196097.532 Hz, Supplied Q-factor (recomputed), Q = 952.822370257, Capacitance to ground, C0 = 3.39318e-15 F.

The next structure is made with 12 fingers. The admittance vs. frequency is shown in Figure 4.9, where the BVD component values are also given.

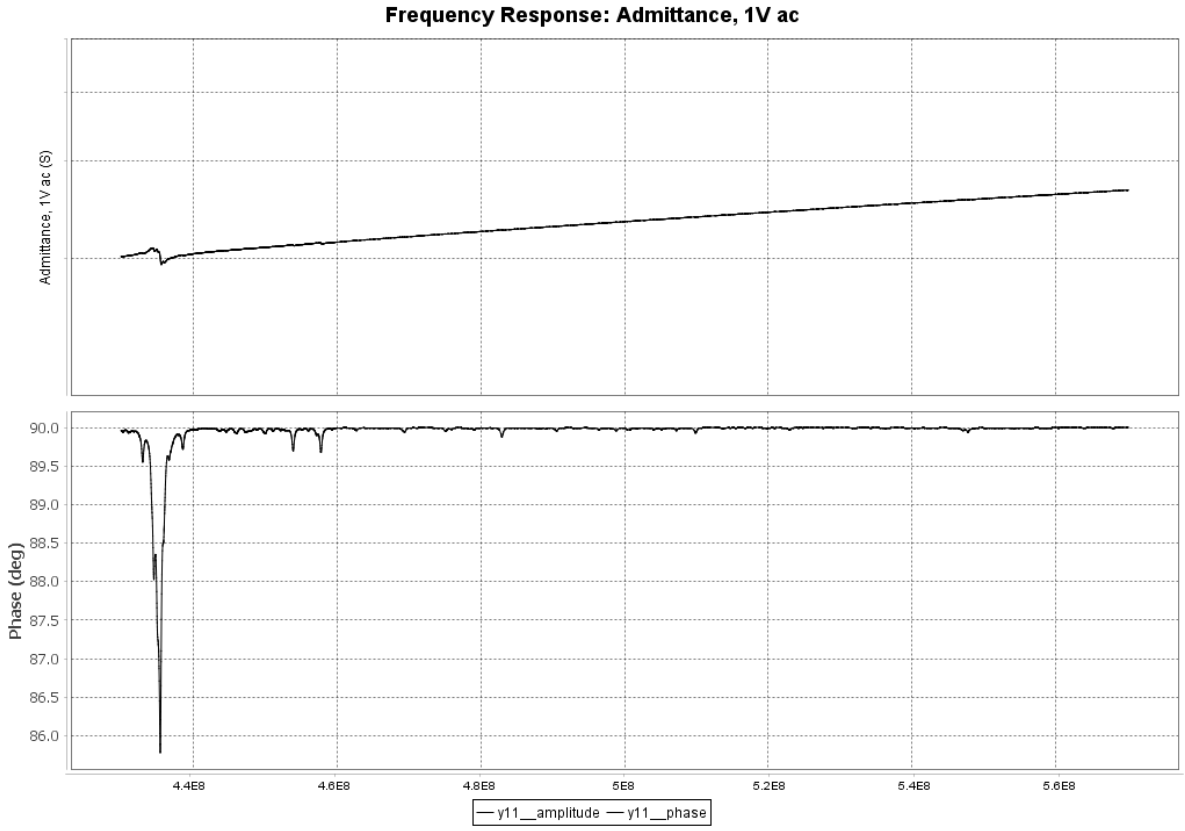

Figure 4.9 Admittance of 12-finger resonator

Motional resistance, Rm = 720928.006162 Ohm, Motional inductance, Lm = 0.242237254005 H, Motional capacitance, Cm = 5.51681198297e-19 F, Series resonance frequency, fs = 435367065.641 Hz, Parallel resonance frequency, fp = 435383227.973 Hz, Supplied Q-factor (recomputed), Q = 919.145951708, Capacitance to ground, C0 = 7.43022e-15 F.

The admittance vs. frequency of the 18-finger resonator is shown in Figure 4.10.

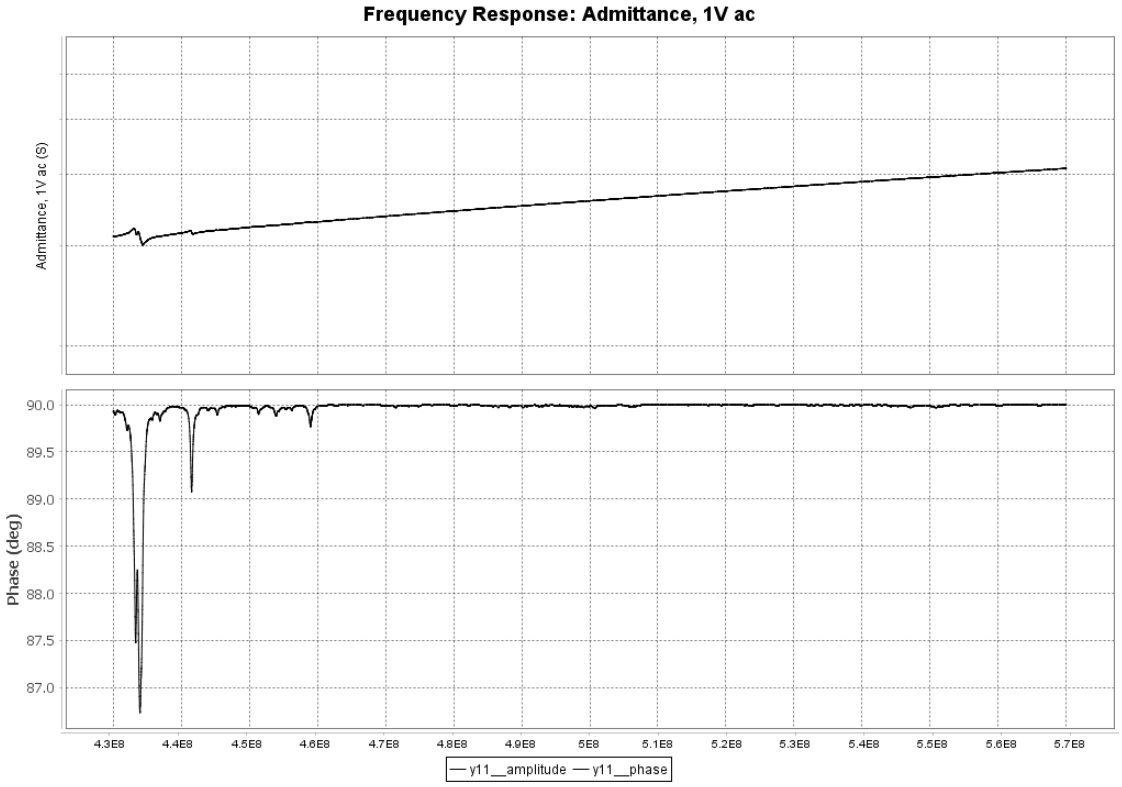

Figure 4.10 Admittance for 18-finger resonator

Motional resistance, Rm = 575169.412577 Ohm, Motional inductance, Lm = 0.11608315587 H, Motional capacitance, Cm = 1.15923351574e-18 F, Series resonance frequency, fs = 433860451.571 Hz, Parallel resonance frequency, fp = 433882385.736 Hz, Supplied Q-factor (recomputed), Q = 550.178172576, Capacitance to ground, C0 = 1.14646e-14 F.

As can be seen in the results listed above, the BVD model components follow a pattern. The following section provides a comparison.

The next step is adding reflectors. Some SAW resonators include reflectors to increase the quality factor. Here, 12 fingers with 6 reflectors on each side are simulated. Figure 4.11 shows the resonator with reflectors.

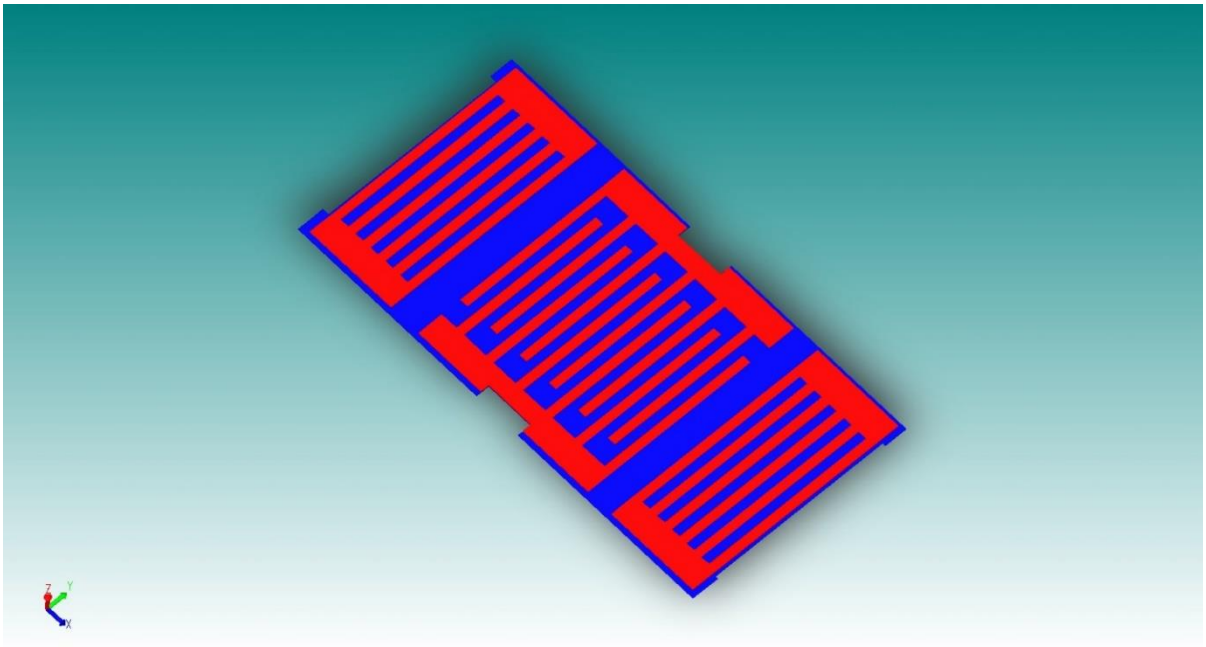

Figure 4.11 Twelve-finger resonator with reflector

According to the simulation results, the Q-factor turned out to be 1089, which is an increase from the original 919. The same procedure was done on an 18-finger resonator with 9 reflectors on each side. In this structure, the simulation showed an increase in the Q-factor. The Q with reflectors turned to be 747, whereas without reflectors it was 550.

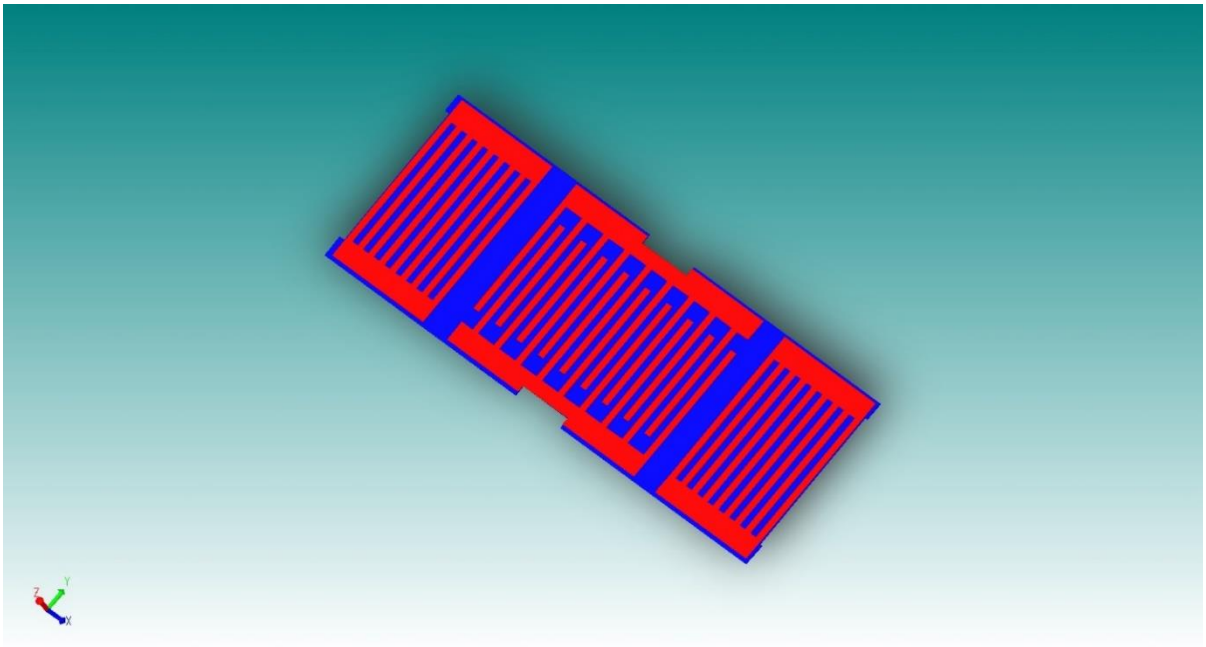

Figure 4.12 Eighteen-finger resonator with reflectors

4.4 Discussion and Comparison

According to the circuit analysis, the relationship between BVD components of different structures was examined to see whether the mechanical simulation is consistent with circuit theory. If the values of BVD components of a single 6-finger resonator are R_m, C_m, L_m and C_o, the values for the BVD components of 6*n fingers will be as follows:

$R_{mn}=R_m/n$, $C_{mn}=n*C_m$, $L_{mn}=L_m/n$ and $C_{on}=nC_o$

So, for 12 fingers and 6 fingers, n is 2. Next, we will check to see whether the values extracted from the mechanical simulation holds for this analysis or not.

In the previous section for 6 fingers, we had:

Rm_6 = 1511939.48778 Ohm, Lm_6 = 0.518522455813 H, Cm_6 = 2.49847414664e-19 F, $C0_6$ = 3.39318e-15 F

where the BVD components for 12 fingers are:

Rm_{12} = 720928.006162 Ohm, Lm_{12} = 0.242237254005 H, Cm_{12} = 5.51681198297e-19 F, $C0_{12}$ = 7.43022e-15 F

So, if we compare them, we get:

Rm_6/Rm_{12}=2.1

Lm_6/Lm_{12}=2.14

Cm_6/Cm_{12}=0.453

$C0_6/C0_{12}$=0.46

Since n=2, the first two equations above should have been 2 and the second should have been 0.5. These figures are very close.

We can do the same with 24 fingers and 30 fingers, with n=1.25.

The BVD values for 24 fingers are as follows:

Rm_{24} = 372894.197319 Ohm, Lm_{24} = 0.0694080140121 H, Cm_{24} = 1.95089915867e-18 F, $C0_{24}$ = 1.55015e-14 F

The BVD values for 30 fingers are as follows:

Rm_{30} = 163072.782878 Ohm, Lm_{30} = 0.0612366389652 H, Cm_{30} = 2.21446136333e-18 F, $C0_{30}$ = 1.9538e-14 F

Similarly, if we compare, we get:

Rm_{24}/Rm_{30}=2.2

Lm_{24}/Lm_{30}=1.15

Cm_{24}/Cm_{30}=0.88

$C0_{24}/C0_{30}$=0.8

Since n=1.25, the first two equations above should have been 1.25 and the second should have been 0.8. Except for Rm, they are very close.

4.5 Circuit vs. Mechanical Analysis

As mentioned previously, the piezoelectric simulation of Coventorware provides BVD circuit components for a SAW resonator. In this section, circuit and mechanical simulation admittance

provided by Coventorware was first shown, as illustrated in Figure 4.13. The purple designates the mechanical simulation result, while the black indicates the circuit component analysis. As can be seen, there is great agreement between the two graphs. Getting the electrical components is very important to predict the filter characteristics with the fabricated filter. The next step is calculating the estimated values for the filter components that were designed and looking at the behavior of the piezoelectric filter in a circuit analysis software like ADS. The designed filter can be seen in Figure 4.14. There are three resonators: two are identical, and one is different. They consist of 260 and 192 fingers, respectively.

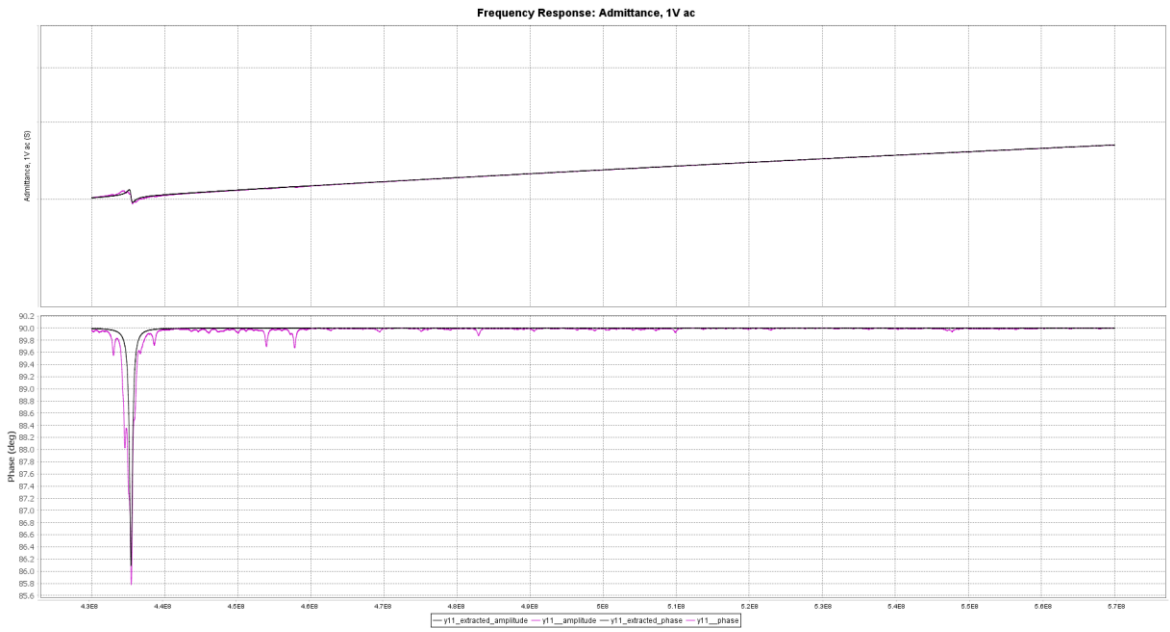

Figure 4.13 Mechanical vs. circuit components

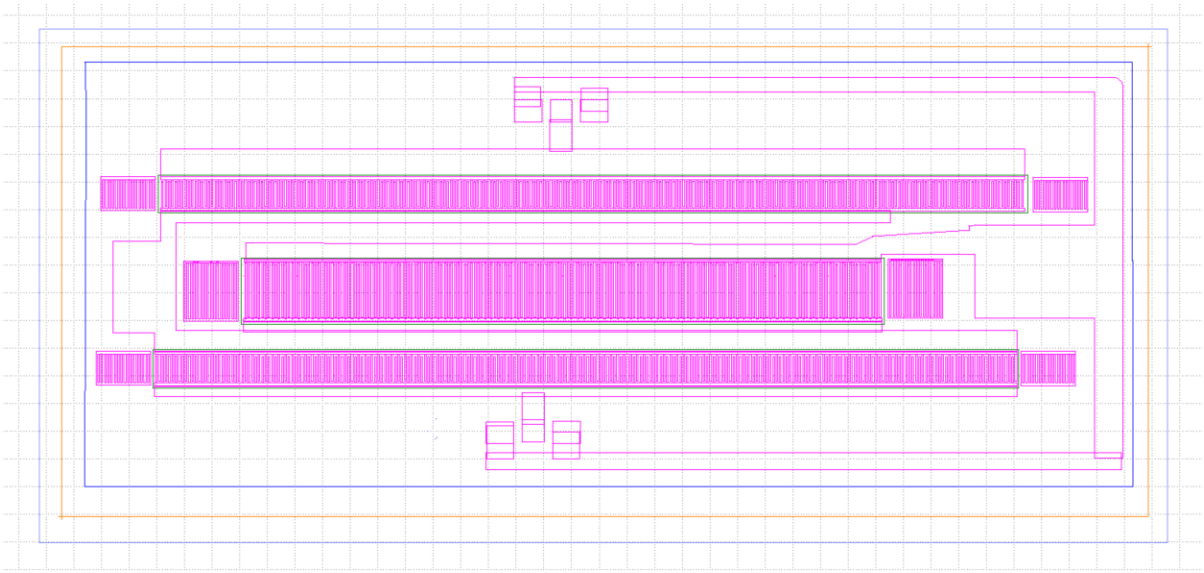

Figure 4.14 Designed filter

The values for the circuit analysis can be calculated through the mathematical and circuit analysis done and shown previously. The 12-finger resonator was used as a reference. The circuit made from the filter and the 12-finger resonator is shown in Figure 4.15.

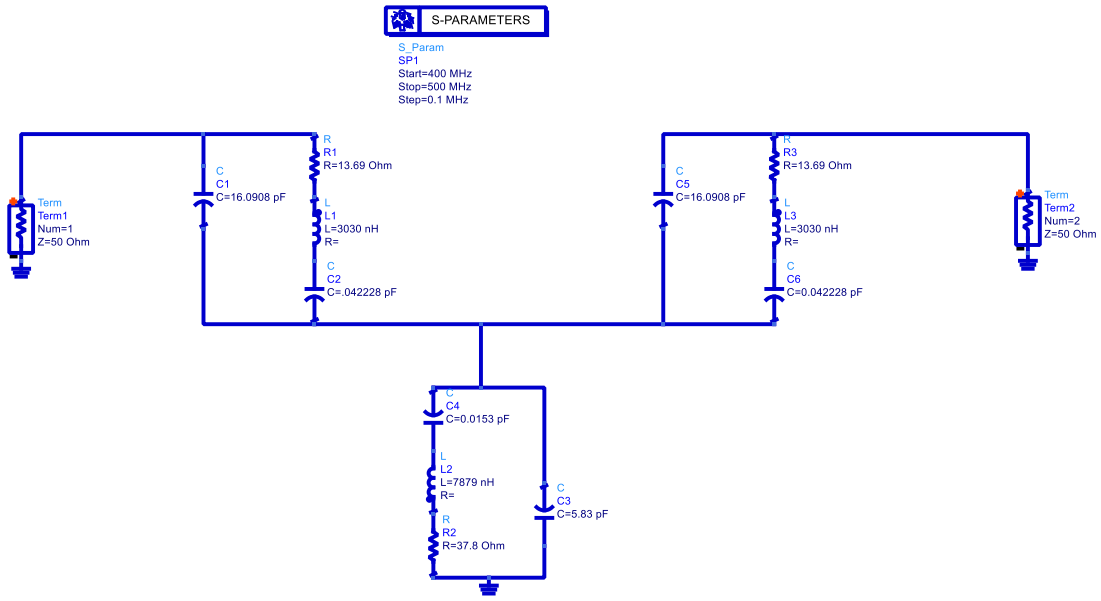

Figure 4.15 Circuit model for the mechanical filter

The values calculated for the 260-finger resonator are as follows:

Co=163e-15 F, Cm=121e-19 F, Lm=0.011 H, Rm=32769 Ohm

Similarly, for 192 fingers:

Co=118e-15 F, Cm=88.32e-19 F, Lm=0.15 H, Rm=45058 Ohm

The circuit behaviour can be seen by S11 in Figure 16. It shows S11 in dB, with a frequency of 435.4 MHz.

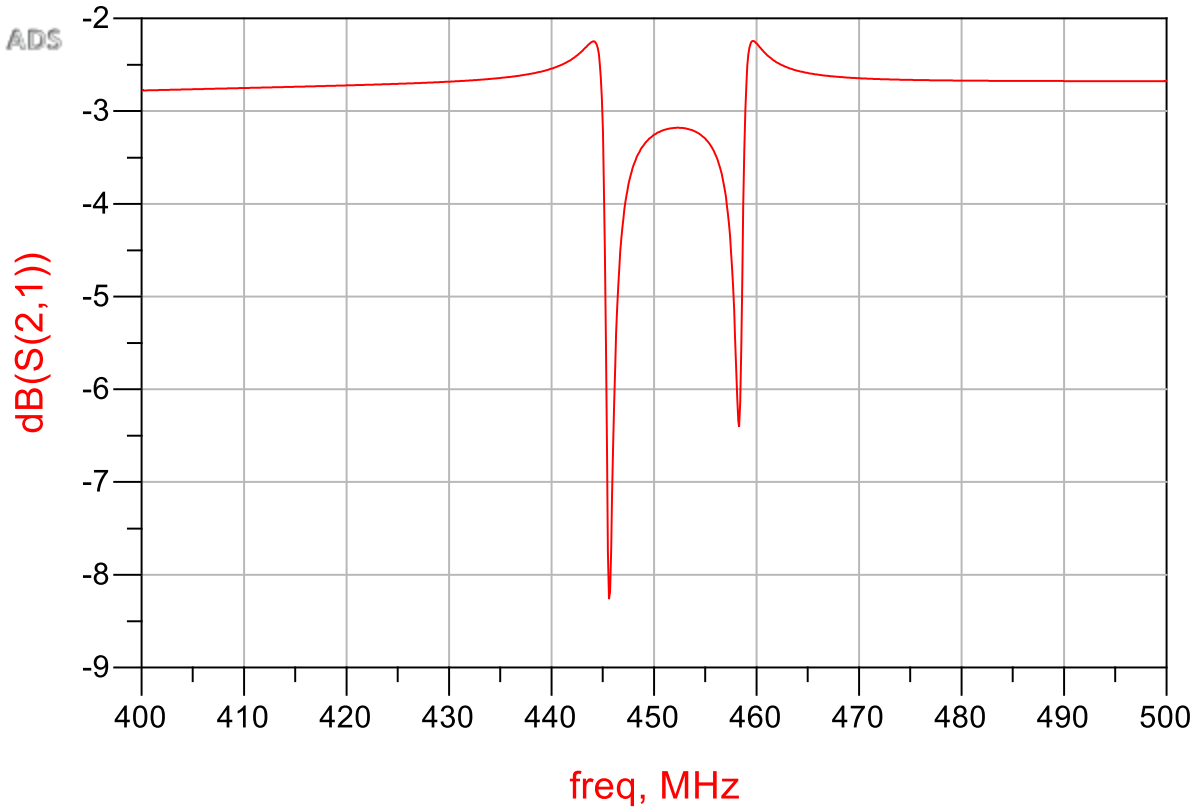

Figure 4.16 S11 of mechanical filter acquired by ADS

4.6 Conclusion

In this study, different surface acoustic wave structures were simulated using the Coventorware fastpze simulation method. The results show the consistency between circuit analysis and mechanical simulation, and an increase in quality factor was seen when reflectors were introduced in the structure. A filter analysis was also performed; however, further investigation is needed.

Chapter 5
Fabrication Measurement Results

5.1 Introduction

After the design was completed using the simulation tools and mathematical analysis, the layouts were done using the KLayout software and the designs were sent through CMC to MEMSPCAP™. After the chips were fabricated and shipped to the Centre for Integrated RF Engineering (CIRFE), they were tested using Agilent PNA. We used a GSG CPW probe.

5.2 Measurement Results

The resonators are designed with three pads that were sized according to the probes. The pads are almost 100 mm^2, and the distance between the center of the pads is around 150 μm. A Scanning Electron Microscope (SEM) image of the designed resonator with 94 fingers is shown in Figure 5.1.

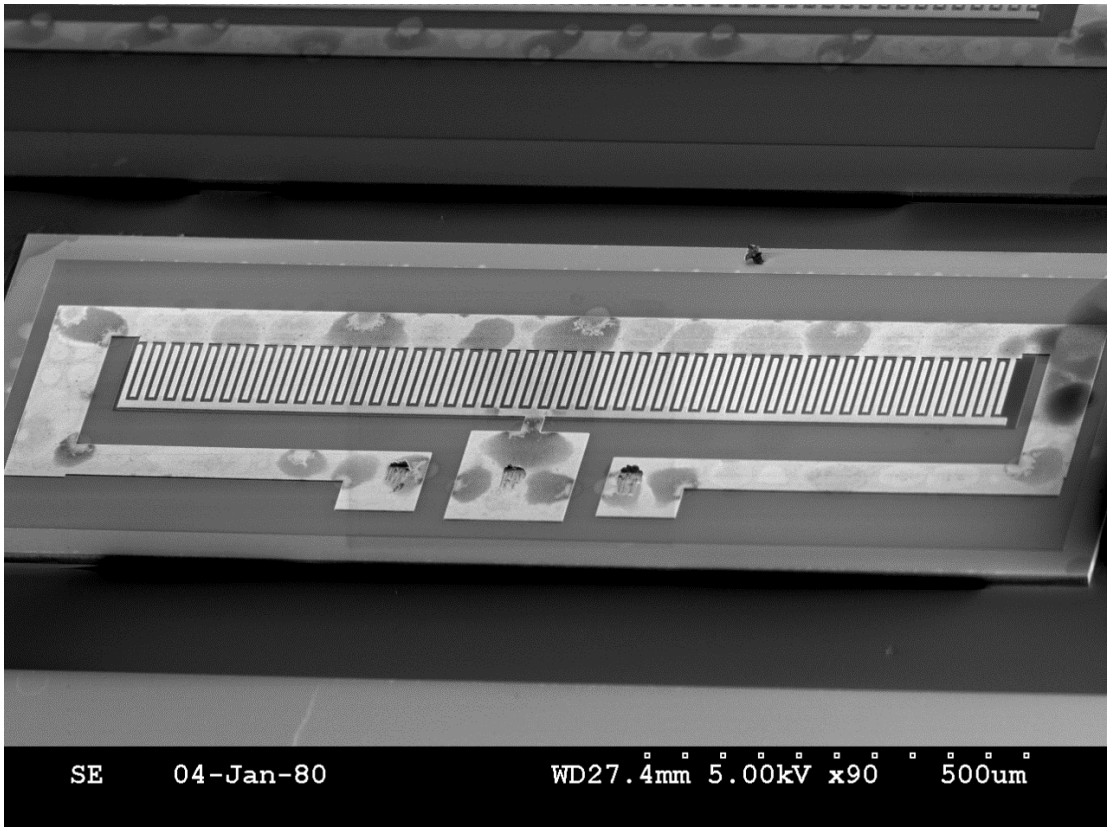

Figure 5.1 SEM image of 94-finger resonator

After the measurements are made on the PNA, the result files are saved as an SnP file and brought back to ADS for further analysis. Since this particular resonator is a one-port device, the s1p file is used for analysis. The log magnitude, phase and Smith chart of S11 can be seen in Figure 5.2, Figure 5.3 and Figure 5.4, respectively. The test frequency sweep is between 10 MHz and 2 GHz with 10,001 points, returning approximately 0.2 MHz steps, which is sufficient for this structure.

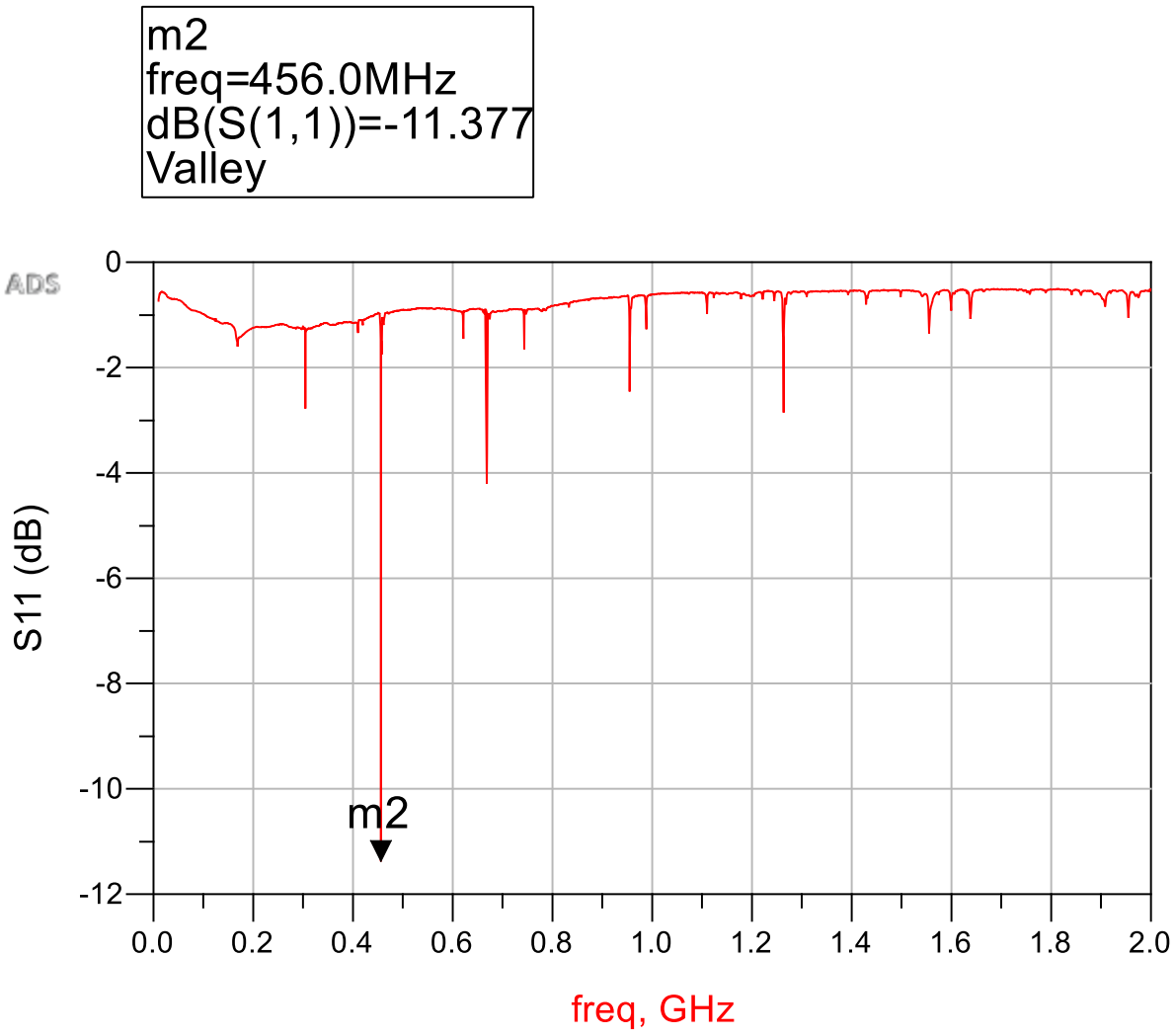

Figure 5.2 S11 (log magnitude) of the 94-finger resonator

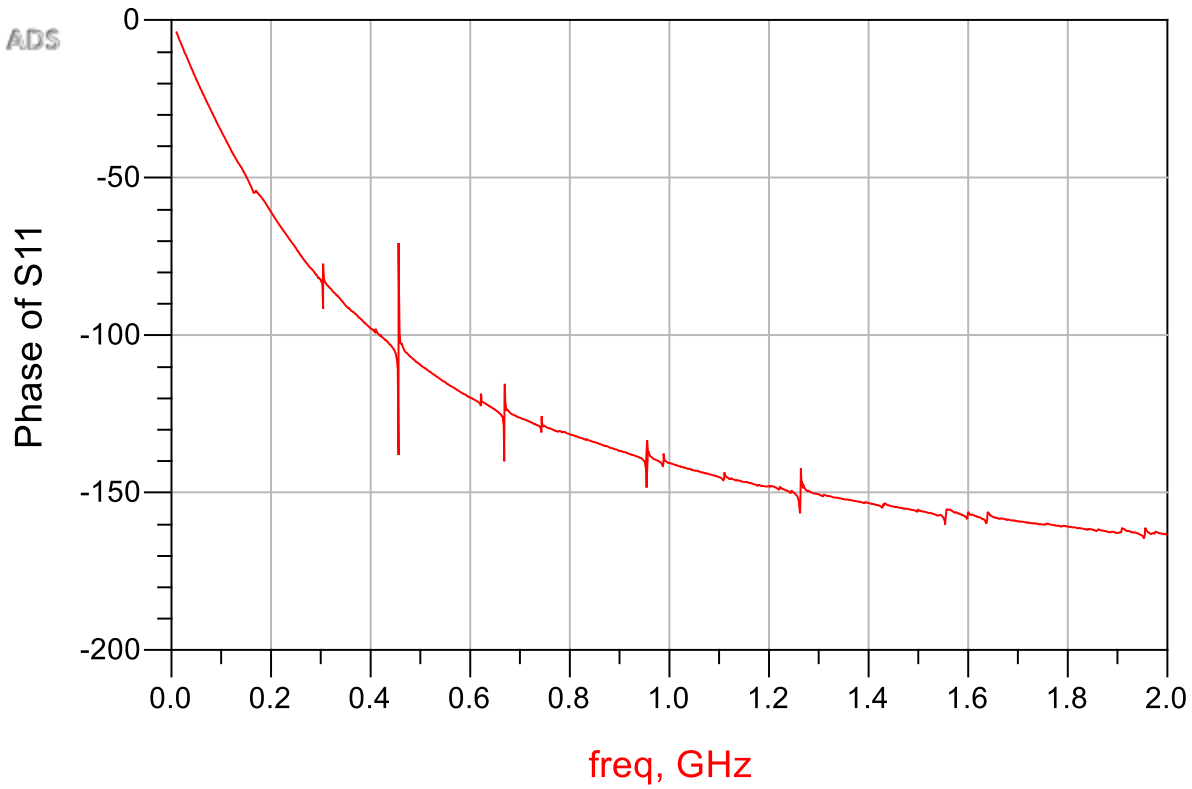

Figure 5.3 Phase of S11 in degrees showing the biggest change around the main resonance frequency

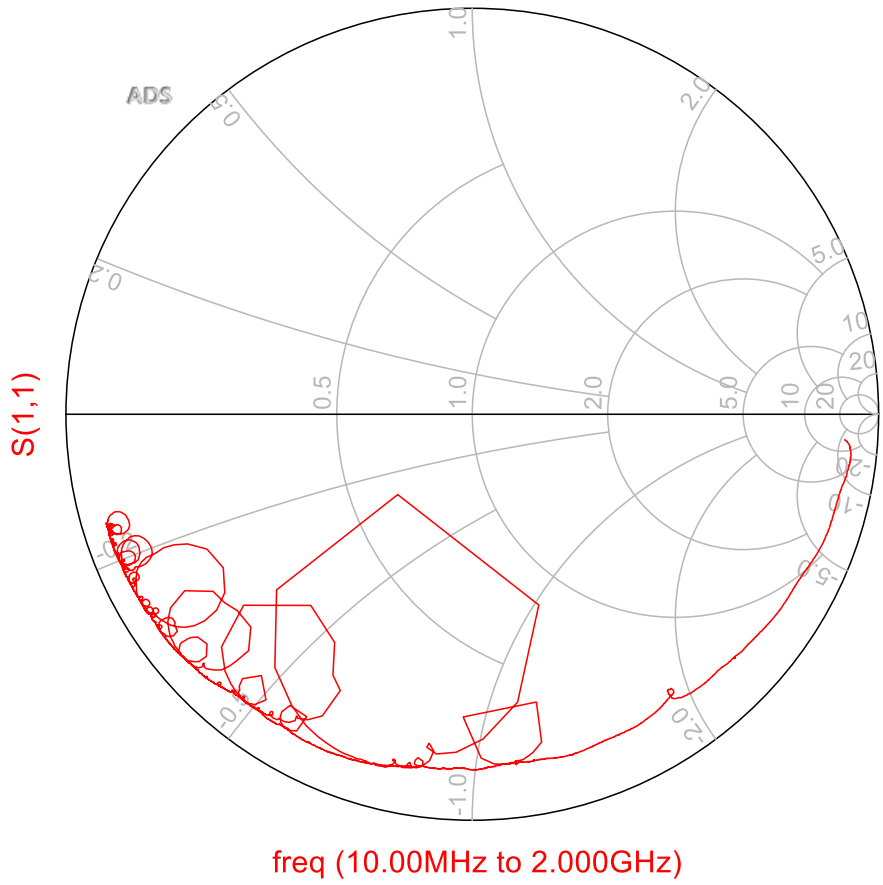

Figure 5.4 S11 on the Smith chart, with each circle corresponding to a certain resonance frequency and the biggest circle being the main resonance

To make things clearer, the S11 dB and S11 phase are shown with a smaller frequency span.

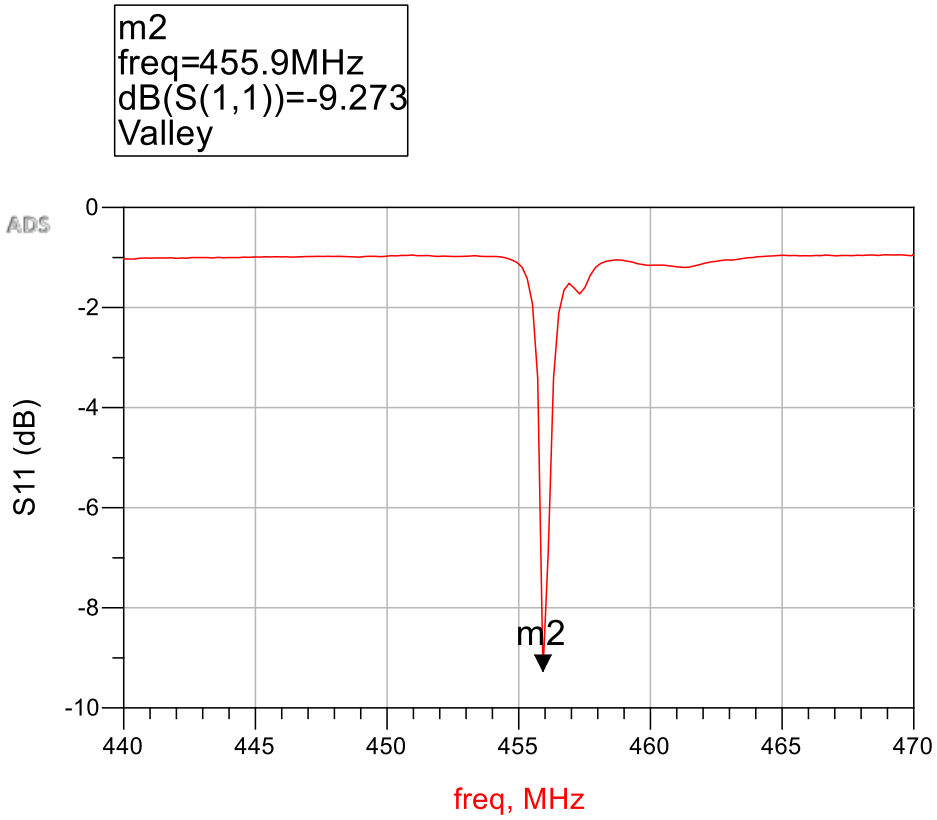

Figure 5.5 S11 dB

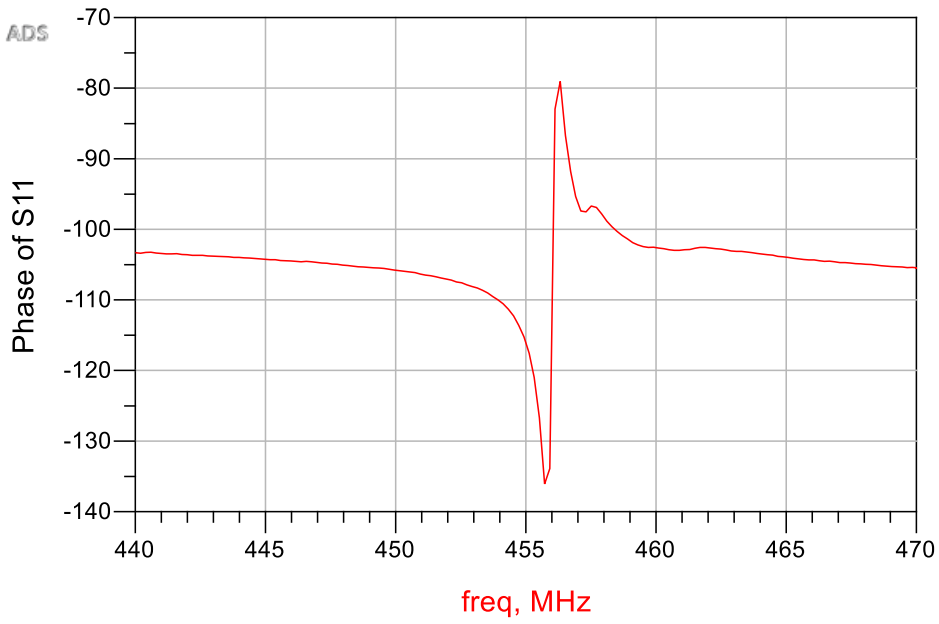

Figure 5.6 S11 phase

In each MEMSCAP run, 15 identical chips are produced and shipped to the designer. The 94-finger resonator was tested on three separate chips and the results were consistent and reproducible. The simulation results obtained from the BVD model shown in Figure 5.7 are compared with measurement results in Figure 5.8.

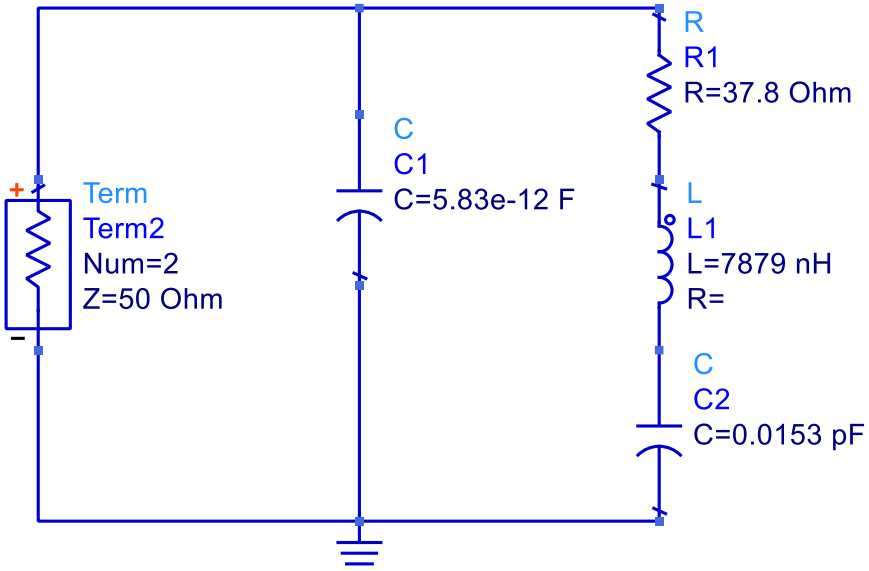

Figure 5.7 BVD circuit model for 94-finger resonator

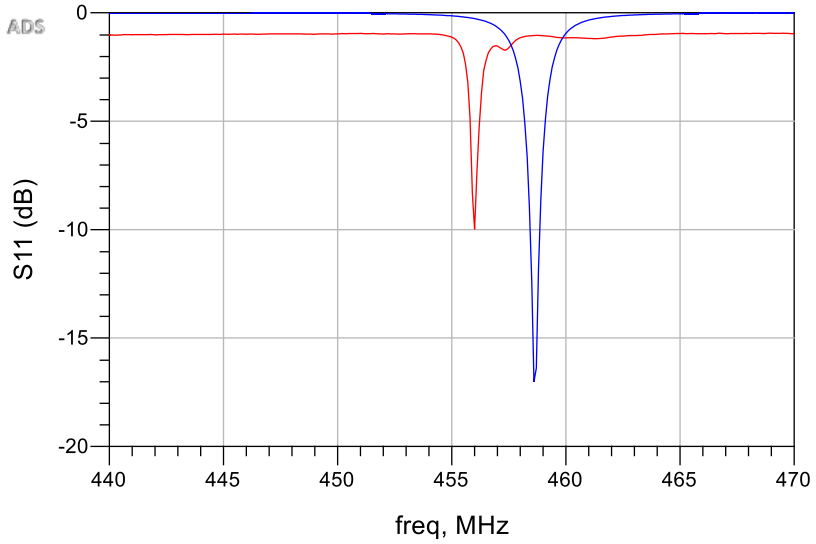

Figure 5.8 S11 (dB) Simulation and fabrication, with the right side being the simulation result of S11, and left side the fabrication result

As can be seen, the simulation and measurement results match perfectly with a difference of only 2.6 MHz, which is less than a 1% error, which shows great accuracy in the mathematical analysis and design procedures. The other two tested resonators showed a similar response but had slightly different resonance frequencies. A summary for the results obtained for the three resonators is shown in Table 5.1.

5.3 Quality Factor

One of the most important aspects of a resonator besides its resonance frequency is its quality factor. This resonator showed a very high quality factor, both loaded and unloaded. The loaded and unloaded were obtained from [31]. Since the resonators are undercoupled, the Q-factor is calculated as follows:

$$Q_L = 10 \log \frac{1+10^{\frac{S11,min}{10}}}{2} \qquad 5.1$$

$$k = \frac{1-10^{\frac{S11,min}{20}}}{1+10^{\frac{S11,min}{20}}} \qquad 5.2$$

$$Q_u = Q_L(1+k) \qquad 5.3$$

Table 5.1 Three Resonators and Comparison Between the Q-Factors

	Resonator 1	Resonator 2	Resonator 3	Simulation
Frequency (MHz)	456	452	442	459.2
Q_L	570	754	803	353
Q_u	882	1349	1424	623
k	0.5584	0.7942	0.7737	0.756

As indicated in Table 5.1, the Q-factors are relatively high and the resonance frequencies are sufficiently close that we can consider the results to be reproducible and consistent.

5.4 Observations

The chip that was designed is shown in Figure 5.9. It has many different resonators with a different number of fingers and one filter having three resonators. However, the difference between the 94-finger resonator and all the other resonators is the use of the TRENCH layer for the mentioned resonator. In the first iteration, we removed this layer from all the resonators except one. The tests results show that the 400 μm thick silicon underneath the structures affects the performance to a great

extent electrically that the results are not even close to what they should be. Consequently, no resonance is seen at the designed frequency.

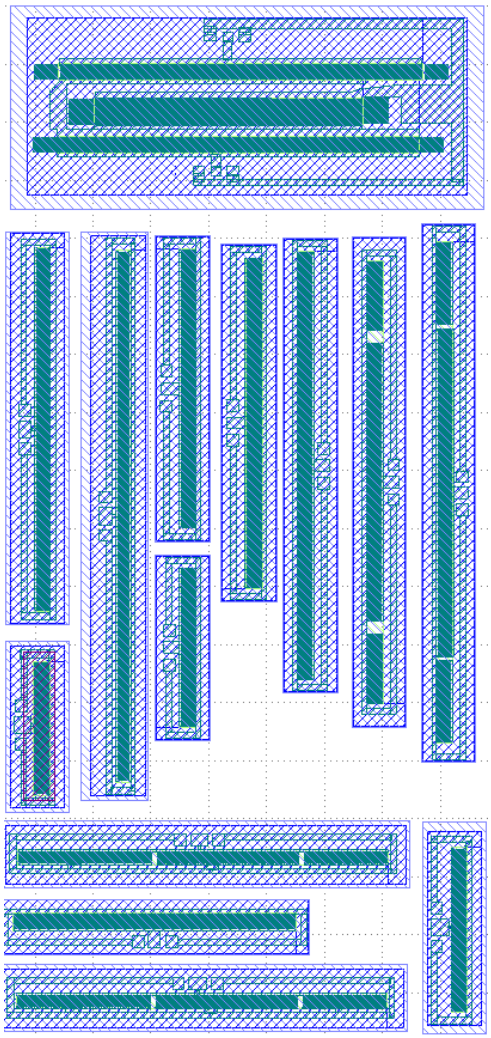

Figure 5.9 The designed layout of different resonators and filter sent to MEMSCAP

As an example, one of the resonators that does not have a TRENCH layer is chosen. This resonator was originally designed to have a 50 Ohm input impedance with 200 fingers and 7.07 pF static capacitance, with a simulated resonance frequency of 450 MHz. The results are shown in Figure 5.10. As can be seen, other than for some spurious modes, there is no significant or meaningful result.

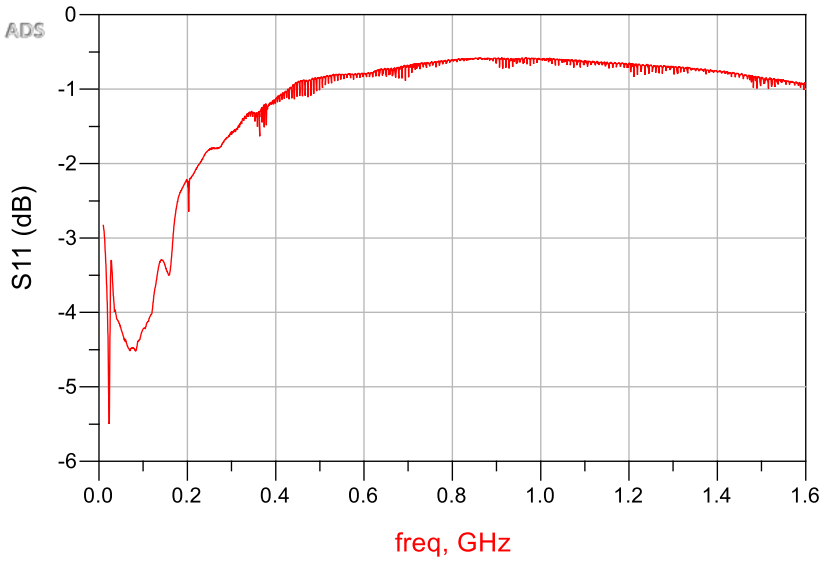

Figure 5.10 50 Ohm 200-finger resonator without TRENCH

5.4.1 Post-process

In order to correct TRENCH layer problem we had in the first design iteration, we tried to add the TRENCH using a silicon etch post-process technique. To create the mask, a very thin layer (approximately 200 nm) of aluminum was deposited on the bottom side of the chip. After the aluminum was deposited, it was patterned using a LASER ablation system. An image of the ablated structure and laser settings can be seen in Figure 5.11. The image shows the procedure done to ablate the backside aluminum using laser. The darker area indicates the bombarded region. The process was very fast and accurate. Following the ablation step, a DRIE system was used to etch through 400 μm of silicon and remove it completely. The mask was only made under the piezoelectric material. After the DRIE (which took around 5-6 hours), the devices were taken to measure and test. Unfortunately, some of the devices were destroyed by the etching process, but some could still be tested. Although they showed great accuracy in the resonance frequency, the device layer was affected by the long amount of time it took to do the etching, so the Q-factor decreased drastically. The dB of S11 can be seen in Figure 5.12. This result is for the 200-finger 50 Ω resonator.

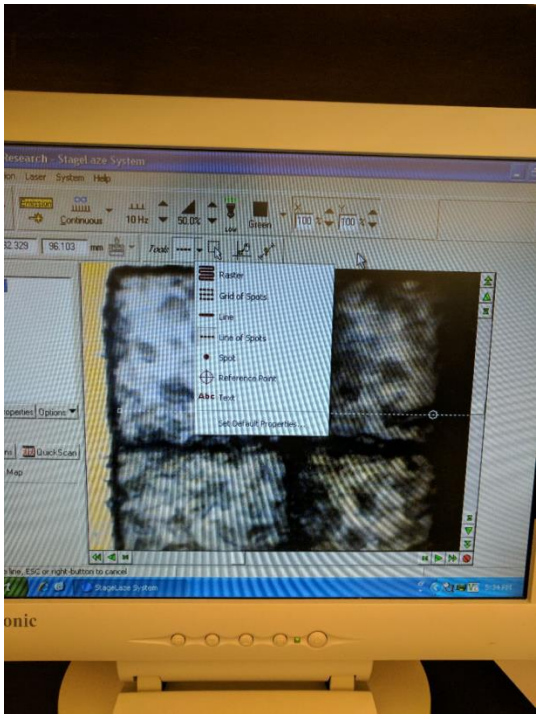

Figure 5.11 Ablated structure

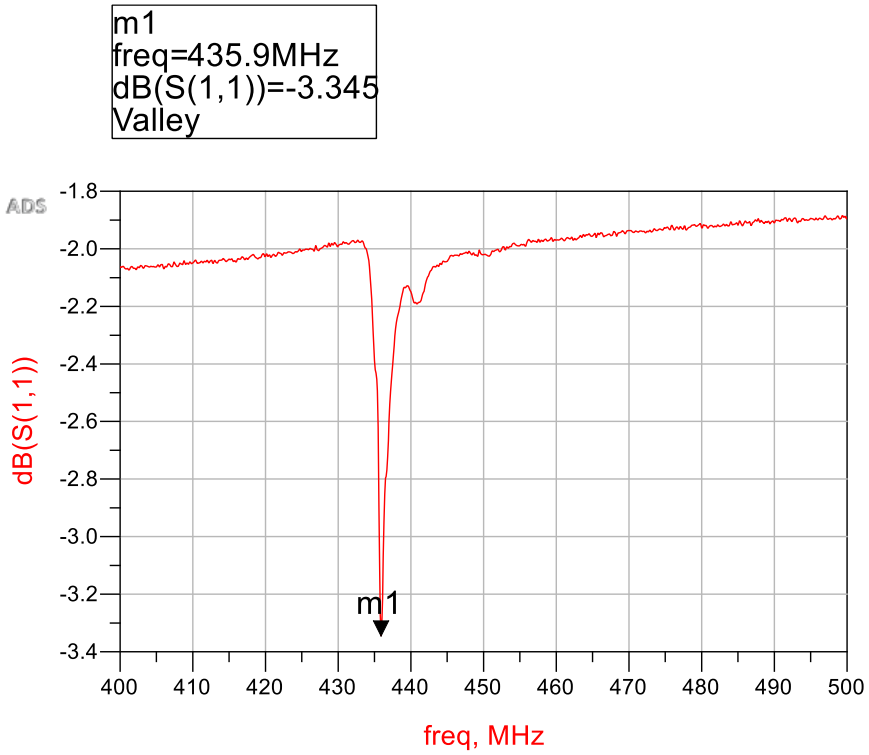

Figure 5.12 S11 (dB) of the 200-finger 50 Ohm resonator

The results could be improved from the earlier ones, but it still needs additional processing. Moreover, there are more chips to do the post-process on.

5.5 Second Run

A new set of resonator elements with built-in trenches was sent to MEMSCAP for fabrication. This run includes some of the resonators from the previous run and a new tunable filter. The layout sent is shown in Figure 5.13.

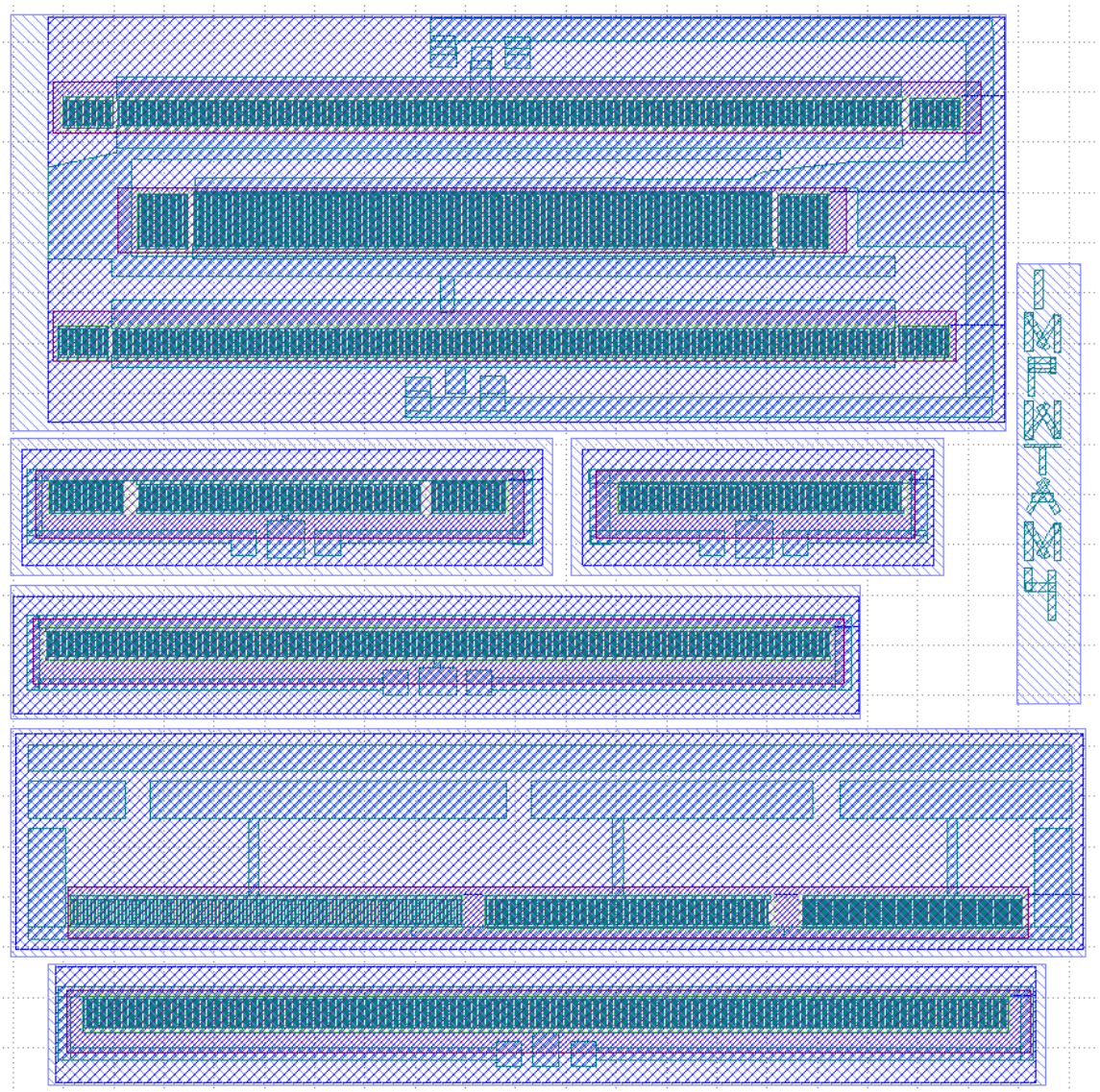

Figure 5.13 Layout sent for fabrication

One of the resonators is the same 94-finger resonator as the one fabricated in the previous run. A version of this resonator included reflectors on each side with 27 fingers to see the effect. The same filter as before, after adding the trenches, was also sent, along with two of the resonators from the previous run (with 260 and 307 fingers). All of these resonators and filters have TRENCH underneath. It was observed that the 94-finger resonator has a response that is consistent with the previous run. The test results show adding reflectors slightly increases the Q-factor. The test results obtained for the 94-finger resonator without and with reflectors are shown respectively in Figure 5.14 and Figure 5.15. With reflectors, Q was increased from 1300 to 1320.

The results for 260 and 307 fingers show a resonance at the designed frequency, however with a much lower Q-factor. Figure 5.16 and Figure 5.17 show the results for the 260-finger and 307-finger resonator, respectively. The respective quality factors are 206 and 56. The reason for this reduction in Q is still under investigation.

The 3-pole filter response was also measured using the PNA. The filter shows high loss in the response. Figures 5.18 and 5.19 show the return and insertion loss, respectively.

Although the filter shows a sort of filtering response, the loss is very high and the filter does not work properly as a result. More investigations are needed to identify the reasons for the high insertion loss and for the deviation of the measured results from the circuit simulation results.

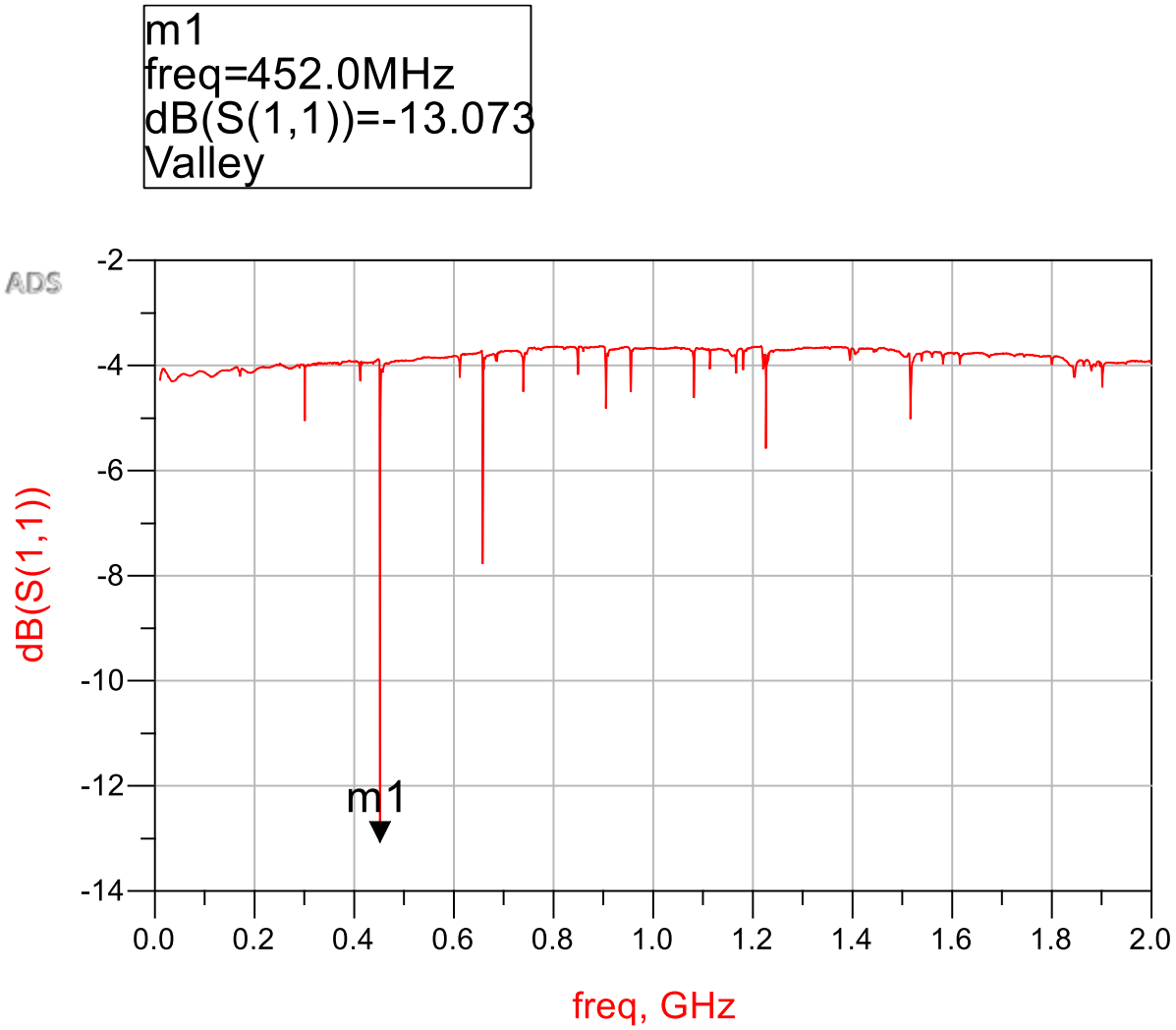

Figure 5.14 Resonator response with 94 fingers

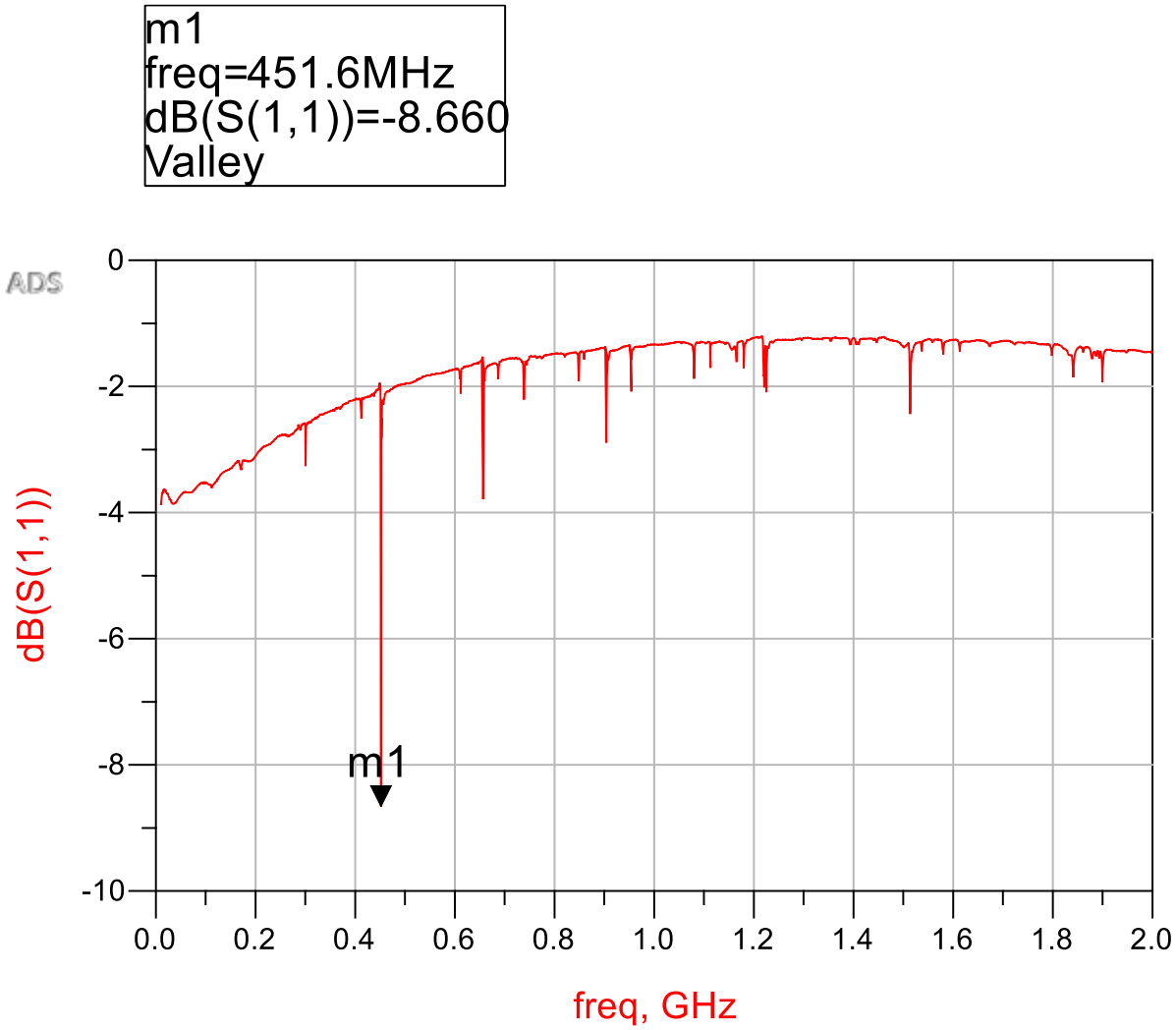

Figure 5.15 Resonator with 94 fingers and reflectors

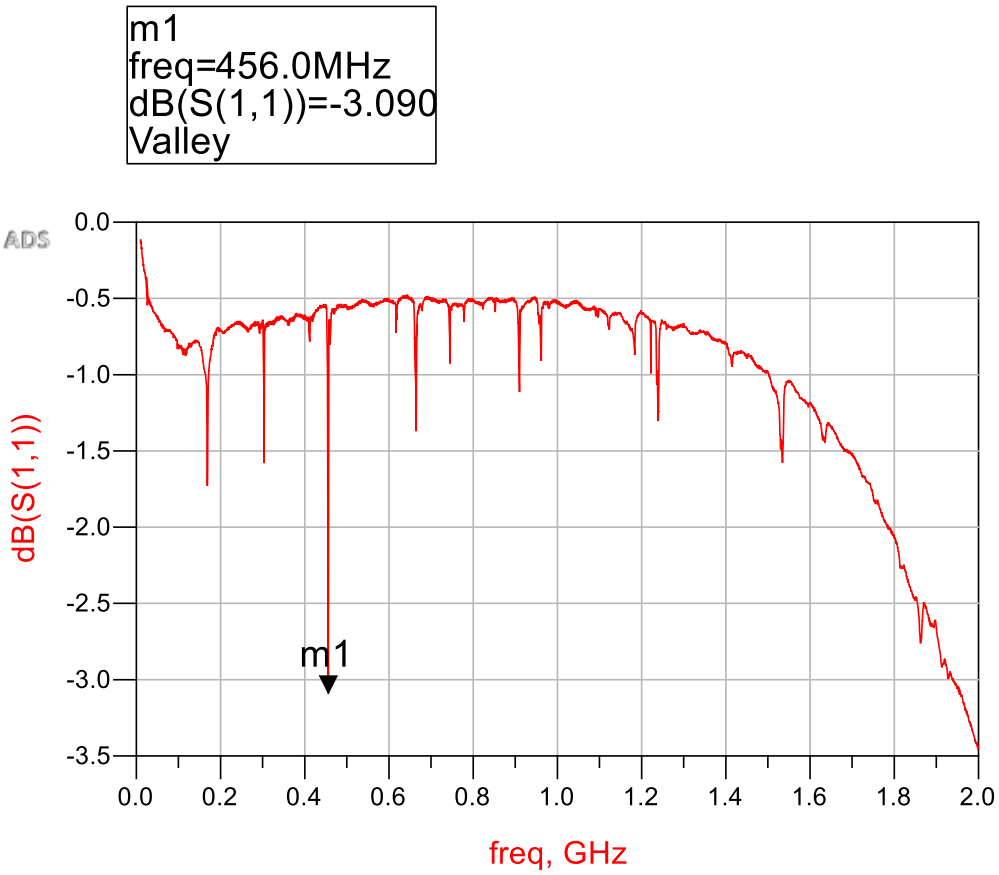

Figure 5.16 Resonator with 260 fingers

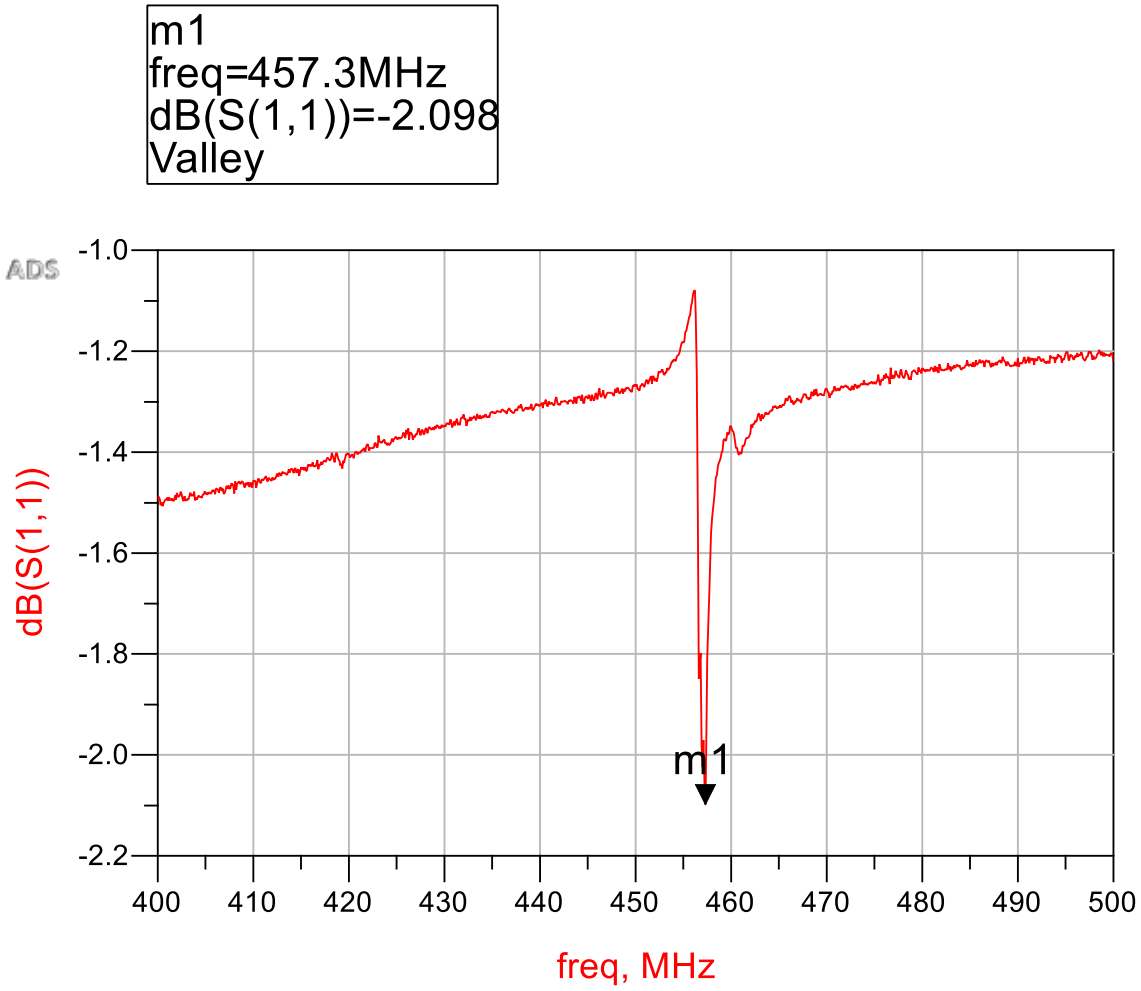

Figure 5.17 Resonator with 307 fingers

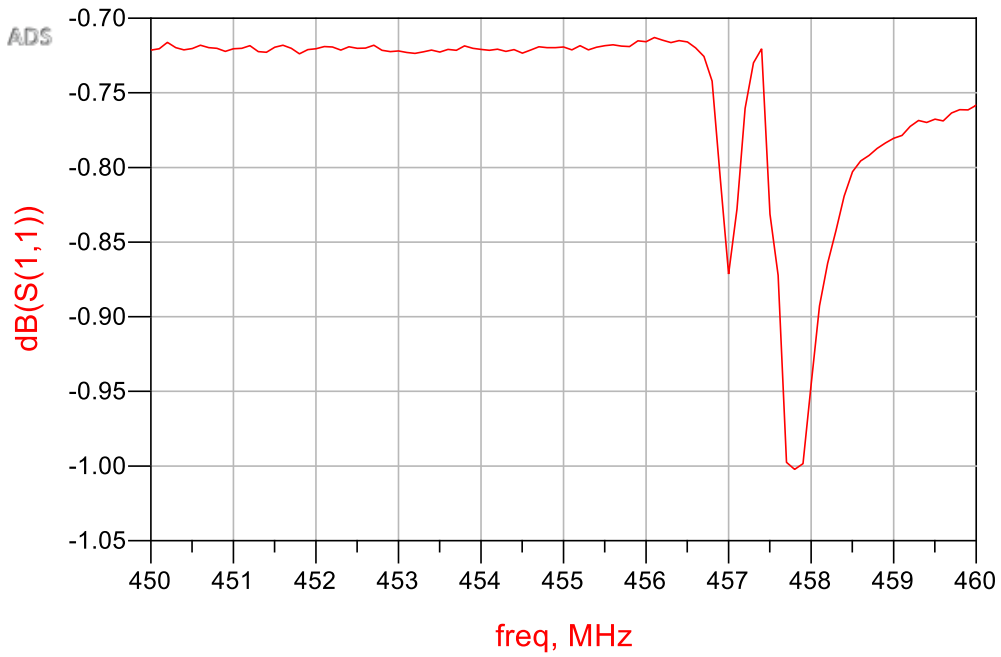

The

Figure 5.18 The filter return loss

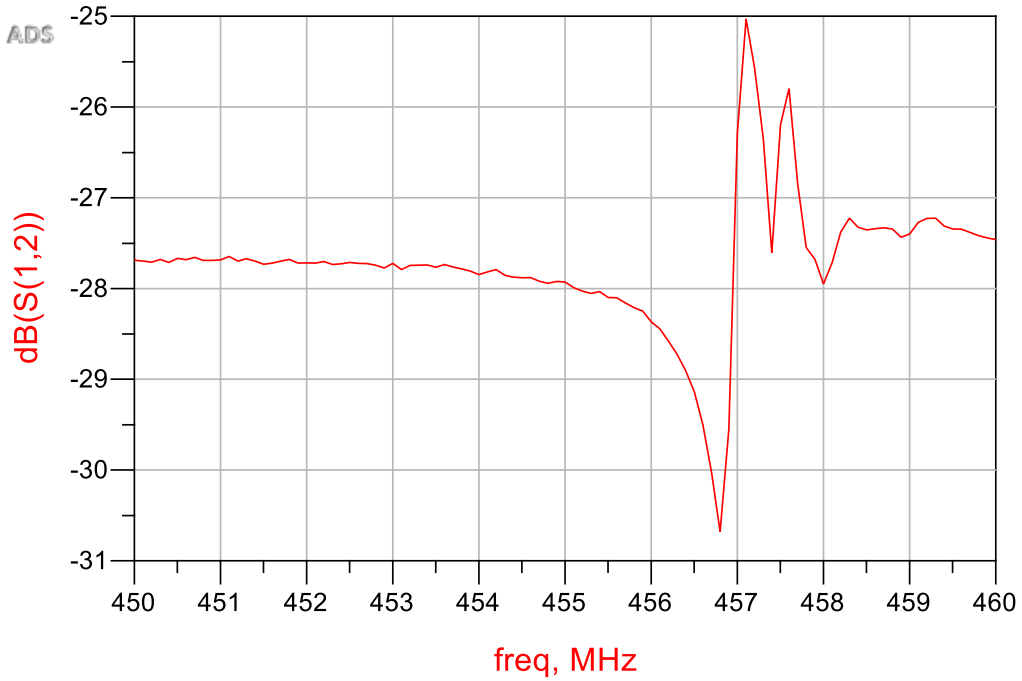

Figure 5.19 Filter insertion loss

Chapter 6
Conclusions

6.1 Contributions

In this study, a fabrication process based on Aluminum Nitride was employed to realize SAW filters and resonators. The quality factor for these resonators proved to be higher than the conventional SAW structures, where Lithium Niobate is mainly used as the piezoelectric. It was shown that PiezoMUMPs is a reliable process to make SAW filters, and that the trench layer plays an important role in the resonator response. Without the trench layer, the bottom silicon acts as a conductor and shifts the resonance frequency drastically. The measured results obtained for some of the resonators fabricated showed a very good match compared to simulations, confirming the accuracy of the mathematical models I implemented. This initial study is certainly not a complete study as it was limited by only two fabrication runs that we could carry out under this MSc program. Further theoretical and experimental investigations need to be carried out to explain some of the unexpected measured results we obtained. Overall, the contributions of this study is it demonstrates the potential of using the PiezoMUMP process in the realization of SAW resonators.

Some of the chips designed in this work were received after the publication of the thesis, so the tests done on those chips will be part of future work. In one of the chips, a 3-pole filter was designed with a provision to add variable capacitors to create a tunable filter. Future work includes study of efficient techniques for realizing SAW tunable filters.

Bibliography

[1] H. P. Loebl, C. Metzmacher, R. F. Milsom, P. Lok, F. van Straten, and A. Tuinhout, "RF Bulk Acoustic Wave Resonators and Filters," *Journal of Electroceramics,* vol. 12, pp. 109-118, 2004.

[2] S. Pourkamali, G. K. Ho, and F. Ayazi, "Low-Impedance VHF and UHF Capacitive Silicon Bulk Acoustic Wave Resonators—Part I: Concept and Fabrication," *IEEE Transactions on Electron Devices,* vol. 54, pp. 2017-2023, 2007.

[3] N. A. Ramli and A. N. Nordin, "Design and modeling of MEMS SAW resonator on Lithium Niobate," in *2011 4th International Conference on Mechatronics (ICOM)*, 2011, pp. 1-4.

[4] J. Zou, "High Quality Factor Lamb Wave Resonators," Research Report, University of California, Berkeley2014.

[5] C. Campbell, *Surface acoustic wave devices and their signal processing applications*: Elsevier, 2012.

[6] A. K. Namdeo and H. B. Nemade, "Extraction of Electrical Equivalent Circuit of One Port SAW Resonator Using FEM-based Simulation," in *Proc. of COMSOL Conference, Pune*, 2015.

[7] B. Donohoe, D. Geraghty, and G. E. O. Donnell, "Wireless Calibration of a Surface Acoustic Wave Resonator as a Strain Sensor," *IEEE Sensors Journal,* vol. 11, pp. 1026-1032, 2011.

[8] K. Jun, S. Kazunobu, and I. Hideharu, "1.5 GHz Low-Loss Surface Acoustic Wave Filter Using ZnO/Sapphire Substrate," *Japanese Journal of Applied Physics,* vol. 32, p. 2337, 1993.

[9] T. Nomura, R. Takebayashi, and A. Saitoh, "Chemical sensor based on surface acoustic wave resonator using Langmuir-Blodgett film," *IEEE Transactions on Ultrasonics, Ferroelectrics, and Frequency Control,* vol. 45, pp. 1261-1265, 1998.

[10] R. Patni, M. Joshi, S. Mehra, and A. Mohan, "Design of Piezoelectric Aluminum Nitride MEMS Resonator," in *Proceedings of the World Congress on Engineering and Computer Science*, 2011.

[11] A. A. M. Ralib, A. N. Nordin, A. Z. Alam, U. Hashim, and R. Othman, "Piezoelectric thin films for double electrode CMOS MEMS surface acoustic wave (SAW) resonator," *Microsystem Technologies,* vol. 21, pp. 1931-1940, 2015.

[12] A. K. Namdeo and H. B. Nemade, "Extraction of COM Parameters and Quality Factor of One Port SAW Resonator using FEM Based Simulation," 2014.

[13] G. Piazza, P. J. Stephanou, and A. P. Pisano, "Single-Chip Multiple-Frequency ALN MEMS Filters Based on Contour-Mode Piezoelectric Resonators," *Journal of Microelectromechanical Systems,* vol. 16, pp. 319-328, 2007.

[14] H. Zhu and J. E.-Y. Lee, "AlN piezoelectric on silicon MEMS resonator with boosted Q using planar patterned phononic crystals on anchors," in *Micro Electro Mechanical Systems (MEMS), 2015 28th IEEE International Conference on*, 2015, pp. 797-800.

[15] G. Piazza, P. J. Stephanou, and A. P. Pisano, "Piezoelectric Aluminum Nitride Vibrating Contour-Mode MEMS Resonators," *Journal of Microelectromechanical Systems,* vol. 15, pp. 1406-1418, 2006.

[16] C. m. Lin, T. t. Yen, Y. j. Lai, V. V. Felmetsger, M. A. Hopcroft, J. H. Kuypers, and A. P. Pisano, "Temperature-compensated aluminum nitride lamb wave resonators," *IEEE Transactions on Ultrasonics, Ferroelectrics, and Frequency Control,* vol. 57, pp. 524-532, 2010.

[17] C. M. Lin, V. Yantchev, J. Zou, Y. Y. Chen, and A. P. Pisano, "Micromachined One-Port Aluminum Nitride Lamb Wave Resonators Utilizing the Lowest-Order Symmetric Mode," *Journal of Microelectromechanical Systems,* vol. 23, pp. 78-91, 2014.
[18] C. Cassella and G. Piazza, "AlN two-dimensional-mode resonators for ultra-high frequency applications," *IEEE Electron Device Letters,* vol. 36, pp. 1192-1194, 2015.
[19] C. Cassella, Y. Hui, Z. Qian, G. Hummel, and M. Rinaldi, "Aluminum nitride cross-sectional Lamé mode resonators," *Journal of Microelectromechanical Systems,* vol. 25, pp. 275-285, 2016.
[20] H. Zhu, C. Tu, and J. E.-Y. Lee, "High-Q low impedance UHF-band AlN-on-Si MEMS resonators using quasi-symmetrical lamb wave modes," in *Micro Electro Mechanical Systems (MEMS), 2016 IEEE 29th International Conference on*, 2016, pp. 970-973.
[21] G. Dhatt, E. Lefrançois, and G. Touzot, *Finite element method*: John Wiley & Sons, 2012.
[22] A. Stefanescu, D. Neculoiu, A. Müller, A. Dinescu, G. Konstantinidis, and A. Stavrinidis, "Analysis of GaN based SAW resonators including FEM modeling," *Romanian Journal of Information Science and Technology,* vol. 14, pp. 334-345, 2011.
[23] P. Smole, W. Ruile, and P. Pongratz, "Characterization of surface acoustic wave propagation in a ZnO layer on a conducting substrate," in *2002 IEEE Ultrasonics Symposium, 2002. Proceedings.*, 2002, pp. 307-310 vol.1.
[24] T. Wada, T. Ogami, A. Horita, H. Obiya, M. Koshino, M. Kawashima, and N. Nakajima, "A new tunable SAW filter circuit for reconfigurable RF," in *2016 IEEE MTT-S International Microwave Symposium (IMS)*, 2016, pp. 1-4.
[25] A. Konno, H. Hirano, M. Inaba, K.-y. Hashimoto, M. Esashi, and S. Tanaka, "Tunable surface acoustic wave filter using integrated micro-electro-mechanical-system based varactors made of electroplated gold," *Japanese Journal of Applied Physics,* vol. 52, p. 07HD13, 2013.
[26] D. Psychogiou, R. Gómez-García, and D. Peroulis, "Continuously-tunable-bandwidth acoustic-wave resonator-based bandstop filters and their multi-mode modeling," in *Microwave Conference (EuMC), 2016 46th European*, 2016, pp. 894-897.
[27] D. Psychogiou, R. Gómez-García, and D. Peroulis, "Acoustic-wave-lumped-element resonator (AWLR) architectures for high-Q reflective bandstop filters," in *Microwave Conference (EuMC), 2015 European*, 2015, pp. 422-425.
[28] A. Cowen, G. Hames, K. Glukh, and B. Hardy, "PiezoMUMPs™ Design Handbook," *MEMSCAP Inc.,* 2013.
[29] J. Pons-Nin, S. Gorreta, M. Dominguez, E. Blokhina, D. O. Connell, and O. Feely, "Design and test of resonators using PiezoMUMPS technology," in *2014 Symposium on Design, Test, Integration and Packaging of MEMS/MOEMS (DTIP)*, 2014, pp. 1-6.
[30] D. Gerlich, S. Dole, and G. Slack, "Elastic properties of aluminum nitride," *Journal of Physics and Chemistry of Solids,* vol. 47, pp. 437-441, 1986.
[31] R. J. Cameron, C. M. Kudsia, and R. R. Mansour, *Microwave filters for communication systems*: Wiley-Interscience, 2007.